FIFTH-ORDER POLYNOMIAL PREDISTORTION FOR MACH-ZEHNDER MODULATOR LINEARIZATION

A Thesis

by

JEFFREY KWABENA OKYERE

Submitted to the Office of Graduate and Professional Studies of
Texas A&M University
in partial fulfillment of the requirements for the degree of

MASTER OF SCIENCE

Chair of Committee,	Samuel Palermo
Committee Members,	Kamran Entesari
	Christi Madsen
	Yoonsuck Choe
Head of Department,	Miroslav M. Begovic

May 2017

Major Subject: Electrical Engineering

ABSTRACT

Modern wireless applications require access to ultra-wide instantaneous RF bandwidths to provide frequency agility and multi-band RF processing. Wireless communications, radar and electronic warfare are examples of applications that will benefit from wideband multi-function transceivers. The role of the front-end filtering is critical in order for the multi-function transceiver to achieve adequate RF performance. Integrated electric filters are unable to achieve the required frequency selectivity and tuning range mainly due to low Q of on-chip inductors. This renders a complete integrated solution impractical. Normally, high frequency and high selectivity filters are achieved with off-chip bulky SAW filters.

The limitation of electrical filters has motivated the employment of RF photonic receivers. The main issue with photonics is the cost but in recent times the emergence of silicon photonics has enabled the potential of RF photonics receivers to be implemented at a low cost. The use of photonics gives access to devices that can achieve really high Q and high integration at high frequencies.

At the heart of the photonic receiver is the Mach-Zehnder modulator (MZM). It modulates the received signal from the antenna to the optical carrier. The major issue with the MZM is: it is non-linear and wideband. The MZM is placed before the photonic filter and right after the antennae so interferers received with the desired RF signal generate intermodulation products at the output of the MZM. The intermodulation products can be very close to the desired RF signal so they cannot be filtered out by the photonic filter and may corrupt the desired RF signal. To curtail the effects of the MZM non-linearity, linearization schemes are implemented to reduce the amplitude of the intermodulation products generated when the MZM receives interferers.

This thesis work focuses on two main issues, Firstly, analysis of the intermodulation products generated by the MZM when a two tone RF signal is applied. Secondly, a literature review is done to examine the existing linearization schemes. Based on the predistortion linearization scheme, a new fifth-order predistortion is proposed. The proposed fifth-order predistortion is fabricated in GP 65nm TSMC CMOS process. The proposed fifth-order linearization achieves high IM3 suppression~ 20dB at high modulation index ~49.7% with 49.2mW of power consumed.

DEDICATION

This work is dedicated to my parents, Philip and Selina Okyere.

ACKNOWLEDGEMENTS

My study in Texas A&M University has been a pleasant one thanks to the kindness of many wonderful people. Firstly, I thank my advisor Dr. Samuel Palermo for agreeing to be my advisor and giving me the opportunity to contribute to RF photonics. In addition to his excellent mentorship and insight, he continuously challenges me to give my best. I sincerely thank Dr. Kamran Entesari, Dr. Christi Madsen and Dr. Yoonsuck Choe for serving as members on my thesis committee. Your time spent and valuable feedback are most appreciated.

My thanks also goes to Tuli Dake, Ben Sarpong, Dee Hunter and Art George all of TI who played a major role in initiating the African University Relations Program (AAURP) through which my masters education in Texas A&M University was made possible.

Finally my thanks goes to my fellow graduates students I worked with in my research group.

CONTRIBUTORS AND FUNDING SOURCES

This thesis work was supervised by a committee consisting of Dr. Samuel Palermo (Advisor), Dr.Kamran Entesari, Dr. Christi Madsen of the Department of Electrical Engineering and Dr.Yoonsuck Choe of the Department of Computer Science.

Under the advisement of Dr. Samuel Palermo of the Department of Electrical Engineering, all the work in the thesis was completed by the student.

Graduate study was supported by a fellowship from Texas A&M University funded by Texas Instrument Incorporated.

TABLE OF CONTENTS

Page

LIST OF FIGURES

Page

LIST OF TABLES

Page

1 INTRODUCTION

Modern wireless applications require access to ultra-wide instantaneous RF bandwidths to provide frequency agility and multi-band RF processing. Wireless communications, radar and electronic warfare are examples of applications that will benefit from wideband multi-function transceivers. For these receivers to have adequate RF-performance, the role of the front-end filtering is critical. The ability of the front-end filter to perform rapid dynamic filtering and interferer cancellation will be essential for the effective use of the ultra-wide band [1], [2].It is challenging for traditional active or passive filters to achieve such level of frequency selectivity, tuning range and speed without trading of size, weight and power target of radio systems. Existing high frequency integrated or on-chip front-end filtering solutions cannot achieve high selectivity and wide tuning requirements necessary for tunable receivers with wide instantaneous bandwidth due to low/moderate on-chip inductor Q factors. Also as these filters are active in nature their linearity is limited. For high selectivity at high frequency off-chip surface acoustic wave (SAW) filters are used which does not provide a complete integrated chip solution.

The limitations of the electrical filters motivates the employment of RF photonic receivers. RF photonic receivers has the advantage of using RF photonic filters. Advancement of silicon photonics has enable the potential of the RF photonic receivers to be implemented in the size, weight and power requirements of radio systems with small form factors[3]–[5]. Silicon photonic filters can achieve Q~200,000 and high integration at high frequencies[6] .

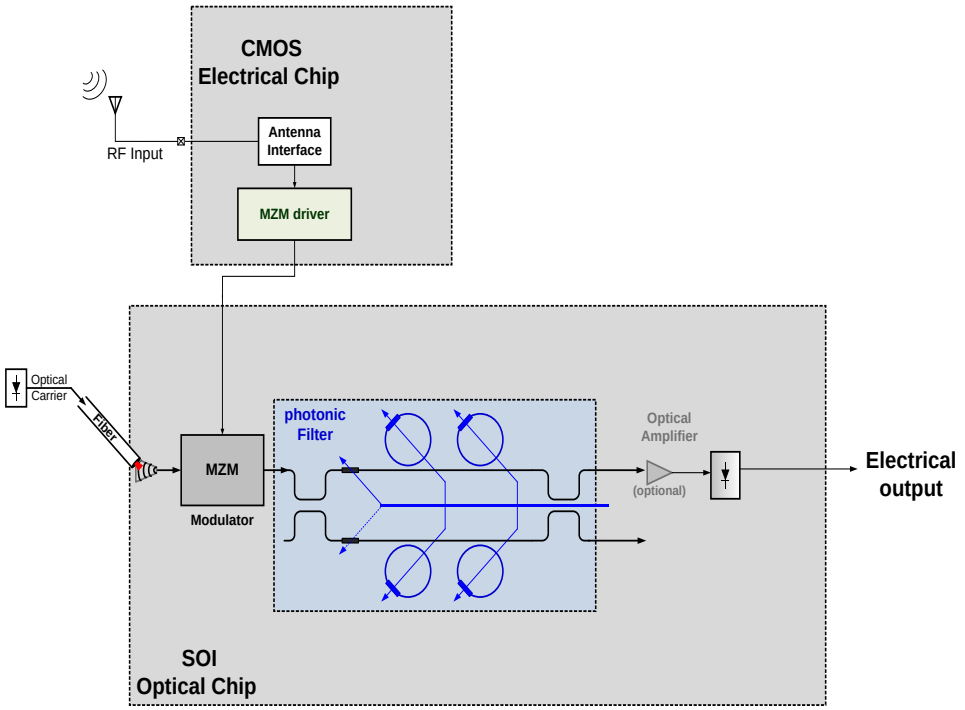

Figure 1.1: Basic silicon photonic RF front-end (RF analog optical link)

At the heart of the RF photonic receiver is the photonic modulator (typically a Mach-Zehnder modulator (MZM)). The MZM modulates the received RF signal from the antenna to the optical carrier and the resulting RF modulated carrier is applied to the filter. The characteristics of the MZM presents a major issue to the RF photonic front-end. The MZM is wideband and inherently nonlinear especially when a large signal is applied to it. The MZM as seen in Fig.1.1 is just after the antennae and right before the photonic filter. In a situation where large blockers are received together with the desired RF signal, they are first applied to the MZM and cannot be filtered out. The blockers can push the MZM to its non-linear region and generate in-band interferers which cannot be filtered by the RF photonic filter resulting in the desired RF signal getting corrupted. This prompts the need for linearization of the MZM. This thesis exams the non-linearity in the MZM and does comparative analysis of existing linearization schemes for the MZM. A proposed linearization of the MZM that

achieves high IM3 suppression~ 20dB at high modulation index ~49.7% is proposed and discussed.

1.1 Organization

In order to understand the non-linearity in the Mach-Zehnder modulator, a proper background in the MZM structure, how it modulates the RF signal onto the optical carrier is important. Chapter II presents a brief overview of existing optical modulators. MZM structure and operation are described. Detailed analysis of the non-linearity of the MZM is presented. Also covered in the chapter are state of the art works in the linearization of the MZM which include both optical and electrical solutions. The merits and demerits of the state of the art works are also discussed.

Chapter III presents the proposed linearization system for the MZM. The individual blocks making the linearizer is discussed. Simulation and experimental results are also presented.

Finally, In Chapter IV a summary of the conclusion of this work is presented.

2 BACKGROUND

The RF analog optical link is composed of a laser source, optical modulator, optical fiber and a photodetector. There are two main approaches of modulating the optical carrier with the RF signals: direct modulation (Fig.2.1) and external modulation (Fig.2.2). Direct modulation involves the modulation signal directly changing the intensity of the laser output. However for external modulation, the laser operates at a constant optical power (CW) and the intensity modulation of the optical carrier is done through a separate device. Although direct modulation is simple in design and low cost, external modulation is more advantageous. External modulation reduces chirp-unwanted wavelength modulation, allows high speed operation and large extinction ratio[7], [8] .

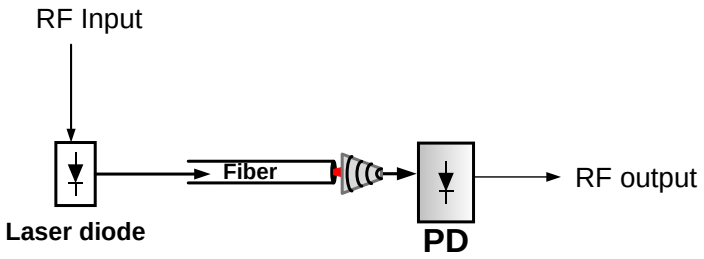

Figure 2.1: Direct modulation

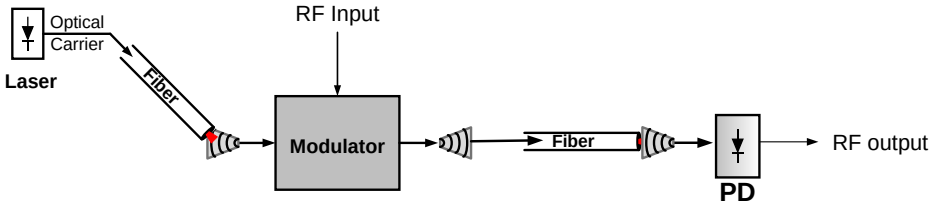

Figure 2.2: External modulation

2.1 Optical Link Components

2.1.1 Optical Modulators

Optical modulators are the heart of the photonic link. They are devices that can alter the parameters of a light source such as amplitude or phase. They modulate the optical carrier with the RF signal. Optical modulators can be grouped into two: direct modulators and external modulators. Direct modulators as the name implies are used for direct modulation. An example is the VCSEL. The external modulator is used for external modulation and examples are EAM, DCM, RRM and MZM.

2.1.1.1 Vertical Cavity Surface Emitting Laser (VCSEL)

A VCSEL is a semiconductor laser that emits light perpendicular to the wafer surface, Fig.2.3. VCSEL are more readily available at short wavelength($0.85\mu m$) [9]where fiber loss is appreciably high. The optical power, P_o and the bias current, I are related by:

$$P_o = \eta(I - I_{th}) \tag{2.1}$$

where η is the slope efficiency and I_{th} is the threshold current. The bandwidth of the VCSEL is directly proportional to the square root of the bias current[10]. VCSELS have the following advantages: they are smaller devices which results in smaller operating current and they can make 2-D arrays. However, they are used for direct modulations so they introduce chirp. In addition, they have sporadic spontaneous emissions which results in amplitude and phase noise at the output light. This is referred to as relative intensity noise (RIN).

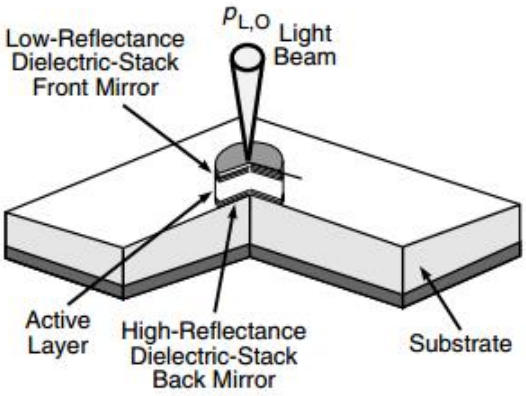

Figure 2.3: VCSEL .Reprinted from[11]

2.1.1.2 Electro-absorption Modulator (EAM)

EAMs are made up of an active semiconductor region sandwich between a p and n- doped layer. They work on the principle known as Franz-keldysh effect[9]. When the voltage applied is zero the EAM is transparent to the laser wavelength but when a sufficient voltage is applied across the p-n layers it becomes opaque and absorbs the wavelength. As the voltage keeps on increasing, there will be a value of voltage where all the wavelength will ideally get absorb. This voltage is referred to as the switching voltage of the EAM. It is normally between 1.5V to 4V[12], [13].The transfer function between the voltage dependent absorption, $\Delta\alpha(v_M)$ and the optical power passing through the modulator, $p_{A,O}$ is given by [14] as:

$$P_{A,O} = T_{FF} P_I e^{-\Gamma L \Delta\alpha(v_M)} \tag{2.2}$$

where Γ is the optical confinement factor, T_{FF} is the loss, P_I is the input optical power and L is the waveguide length.

EAMs are advantageous because they are small in size. In addition, they can be monolithically integrated on the same substrate with a CW DFB laser which results in a compact design and low coupling loses between the two components. The problem associated with EAM is: it introduces some chirp. Although the chirp introduced by an EAM is not as large as the one introduced by direct modulation (VCSEL), it may still be significant depending on the application. The EAM's chirp is generated because the electric field applied modulates both the absorption characteristics and the refractive index of the EAM [9]. Another issue with EAM is the Franz-keldysh effect is very weak in silicon so EAM is not used if the photonic link should be of silicon.

2.1.1.3 Directional Coupler Modulator (DCM)

The DCM consist of two waveguides place next to each other with electrodes alongside them. The arrangement is then fabricated on an electro-optic material such as lithium niobate, Fig.2.4. The DCM works on the operation of evanescent coupling. The spacing between the two waveguide is such that when no voltage is applied, all the optical power in one of the incident waveguides ideally transfers to the other waveguide output. When the voltage applied to the electrode is increased the electric field changes the refractive index which in turn changes the coupling length such that some of the optical power stays in the incident waveguide to the output. At sufficiently high voltage called the switching voltage, all the optical power will ideally stay in the incident waveguide to the output. The transfer function between the electrode voltage,v_M and the optical output, $p_{D,0}$ is given in [15] as:

$$p_{D,O} = T_{FF} P_I \frac{sin^2\left(\frac{\pi}{2}\sqrt{1+3\left(\frac{v_M}{Vs}\right)^2}\right)}{\sqrt{1+3\left(\frac{v_M}{Vs}\right)^2}} \tag{2.3}$$

where P_I is the input optical power, T_{FF} is the insertion loss and V_S is the switching voltage.

DCMs are sensitive to fabrication errors. This is because the coupling strength can be very sensitive to the coupling spacing. To get the exact coupling spacing during fabrication is challenging because of the size of the coupling spacing (tens of nm).

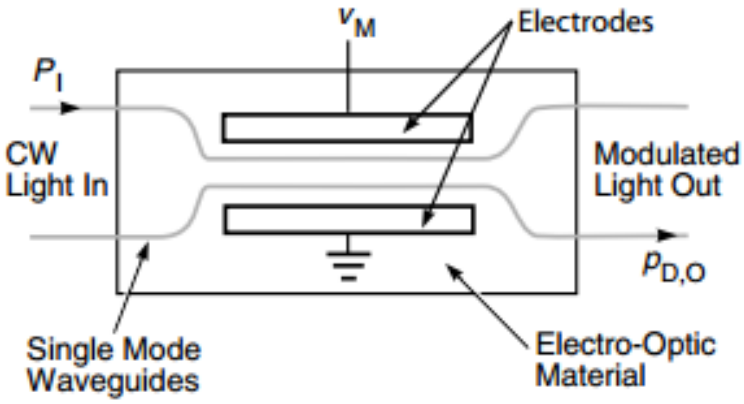

Figure 2.4: DCM Reprinted from[11]

2.1.1.4 Ring Resonator Modulator (RRM)

A ring resonator is a loop structure constructed from a waveguide. In order to be used for optical modulation, it is coupled to a straight waveguide as shown in Fig.2.5. In some applications, the straight waveguide is more than one .RRMs are refractive devices with high quality factor. When the optical source is applied to the input port, part of the optical source travels through to the output port and part of it is coupled into the ring. The transmission power P_{t1} at the output of the waveguide is given as [16]

$$P_{t1} = \frac{\alpha^2 + |t|^2 - 2\alpha|t|cos(\theta + \psi_t)}{1 + \alpha^2|t|^2 - 2\alpha|t|cos(\theta + \psi_t)} \tag{2.4}$$

where α is the loss coefficient of the ring, $|t|$ represents the coupling losses and ψ_t the phase of the coupler. The amount of the optical source coupled into the ring is controlled by altering the refractive index of the ring waveguide. The refractive index of the ring waveguide is altered by the electrical signal applied to it. At a certain electrical signal level resonance occurs and more of the optical source get coupled into the ring and the amount transmitted greatly reduces. At resonance, $(\theta + \psi_t) = 2\pi m$, where m is an integer, the transmission power reduces to: [16]

$$P_{t1} = \frac{(\alpha - |t|)^2}{(1 - \alpha|t|)^2} \tag{2.5}$$

When the internal loss is equal to the coupling loss that is $\alpha = |t|$ the transmitted power becomes zero at resonance. RRMs are able to support multiple resonances which are spaced at wavelength intervals called free spectral range (FSR). The ring resonator modulator has a relatively small size (ring diameter$< 25\mu m$) that makes it really attractive. In addition, it can be used to implement add and drop filters which are very useful in applications such as dense wavelength division modulation(DWDM) The main issue of the RRM is its high sensitivity to wavelength.

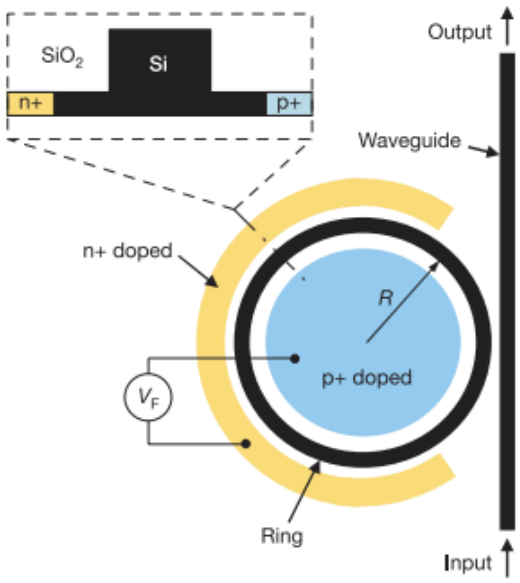

Figure 2.5: Schematic layout of RRM. Reprinted from[17]

2.1.1.5 Mach-Zehnder Modulator

The Mach-Zehnder modulator (MZM) works on the principle that when an electrode is placed on a material like lithium niobate, the electric field generated by the electrode when a voltage is applied to it alters the index of refraction of the lithium niobate. The phase of an optical wave passing through it is thus altered. The MZM is made up of optical waveguide with electrode placed alongside it. A typical layout of an MZM is shown in Fig.2.6.The waveguides all propagate a single spatial optical mode [11]. A CW laser is applied at the input. The CW laser as it passes through the MZM is split equally and it is applied to two arms which are normally of the same length and have their output recombining to feed the output of the modulator. When the voltage applied to the electrode is zero, the light in both paths will ideally travel at the same speed and then recombine in phase at the output of the MZM as shown in Fig.2.7 (a). Maximum optical power is transmitted through the modulator under this condition. When a voltage is applied, an electric field is generated which is perpendicular to the waveguide thus altering the refractive index

in the two arms. The voltage applied to the center electrode causes the index of refraction to increase in one arm and decrease in the other arm because the electro-optic effect is field direction dependent with respect to the propagation axes [11]. The change of index of refraction results in a relative phase shift between the light in the two arms when they combine, Fig.2.7 (b). The combination of the out of phase beam turns to generate higher modes but because the wave guide is single mode these high modes are lost to the surrounding substrate through scattering. Therefore as the voltage increases, the intensity in the output decreases. At a sufficiently high voltage the phase difference of the light in the two arms become exactly 180°. Ideally under this condition the light at the output of the MZM will be zero. Increasing the voltage further will begin to bring the light in the two paths in phase. As a result, the MZM transfer function between the voltage applied to the electrodes and the output optical power is periodic in nature. The MZM transmission as a function of applied voltage (V) is given by[18]:

$$P_{m,out}(\lambda) = \frac{T_{FF}P_{in}}{2}\left[1 + cos\left(\frac{\pi V}{V_{\pi}(\lambda)} + \varphi_b(\lambda)\right)\right] \tag{2.6}$$

where $P_{m,out}$the output is optical power, P_{in} is the input laser power, T_{FF} represents the insertion loss. A typical value is 3dB to 5dB for lithium niobate MZM. V_{π} is the voltage required to induce a 180° phase shift between the two arms and φ_b is the modulator phase bias. φ_b is a function of the wavelength and it is given as[18] :

$$\varphi_b = 2\pi\frac{\Delta nL}{\lambda} + \pi\frac{v_M}{V_{\pi}} \tag{2.7}$$

where ΔnL the internal length is mismatch between the two arms $(n_1L_1 - n_2L_2)$, λ is the optical wavelength in a vacuum and v_M is the external applied voltage. V_{π} is

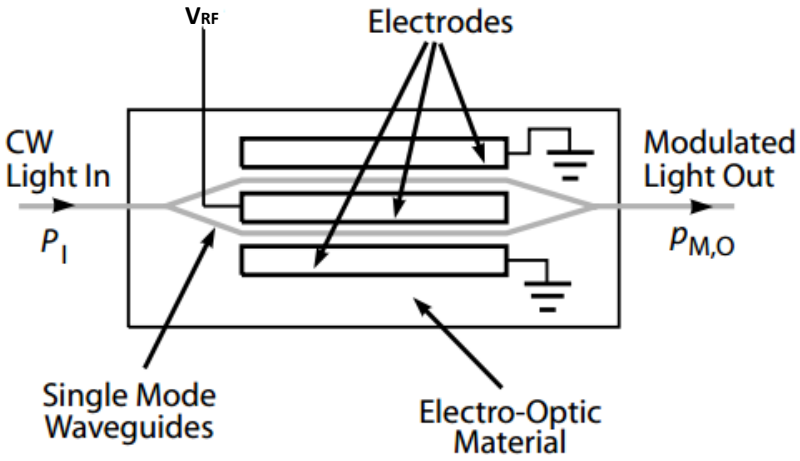

Figure 2.6: Layout of MZM. Reprinted from[11]

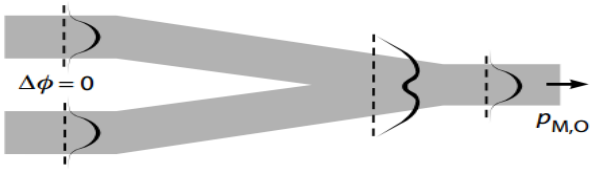

(a) Reprinted from[11]

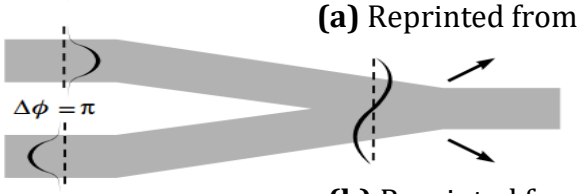

(b) Reprinted from[11]

Figure 2.7: (a), (b) MZM with 0 and π phase shift respectively

an important parameter of the MZM. It determines the modulation efficiency. V_π is set by the physical structure of the MZM. It is given as [18]:

$$V_\pi(\lambda) = \frac{\lambda d}{2\Gamma(\lambda) n^3(\lambda) r(\lambda) L_m} \tag{2.8}$$

where d is electrode separation; L_m electrode length, $\Gamma(\lambda)$ confinement factor $n(\lambda)$ is the index of refraction and $r(\lambda)$ is the electro optic coefficient.

The bias voltage v_M is chosen such that the MZM is biased at the point where it is most linear. This point is normally referred to as the quadrature point (Fig.2.8). It is important to bias the MZM at this point especially when the MZM is used in an RF (analog) communication. For the MZM to be bias at this point requires:

$$\phi_b = \frac{(2k+1)\pi}{2}, k = 0,1,2, \ldots \tag{2.9}$$

From (2.7),ΔnL is very small so can be neglected. (2.7) becomes:

$$\varphi_b \approx \pi \frac{v_M}{V_\pi} \tag{2.10}$$

From (2.9) and (2.10) the bias voltage required for the MZM to be bias at the quadrature point is given as:

$$v_M \approx \frac{(2k+1)}{2} V_\pi, k = 0,1,2 \ldots \tag{2.11}$$

$$For\ k = 0, \qquad v_m \approx \frac{V_\pi}{2} \tag{2.12}$$

Another important parameter of the MZM when used in RF application is the 1-dB compression point. 1-dB compression point of the MZM is the RF signal level at which the gain of the MZM will deviate from its ideal (small signal) value by 1dB. The 1-dB compression point is important because it gives a measure of the input RF signal level beyond which the signal generated at the output of the MZM will begin to see significant distortion. The 1-dB compression point in terms of peak voltage is given as [19]:

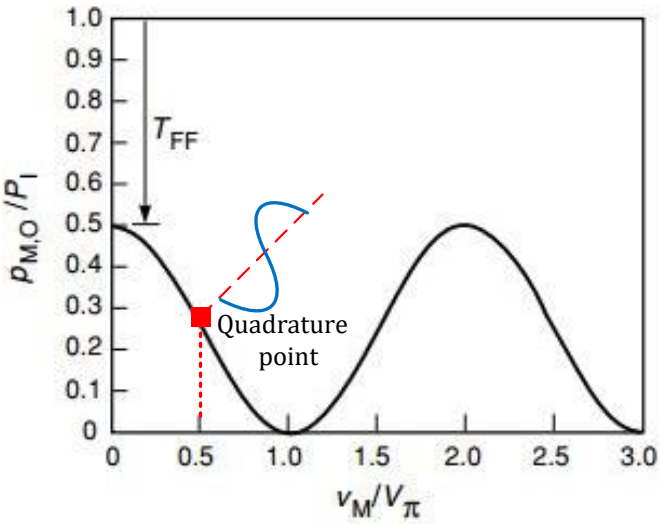

Figure 2.8: MZM transfer function

$$v_{1-dB} \approx \frac{V_\pi}{\pi} \tag{2.13}$$

Next is to look at the frequency response of MZM. The MZM's frequency response is independent of the bias voltage and it is characterize by the ratio of the optical transit time past the electrodes relative to the modulation period of the maximum modulation frequency. At relatively low modulation frequencies, the modulation signal is essentially constant during the optical transit time. This is because the optical transit time is much shorter than the modulation frequency. Under such condition the electrode can be treated as a lumped capacitance and the 3dB corner frequency is set by the lumped electrode capacitance and the 50ohm matching resistance. Typical electrode capacitance of lithium niobate modulator is 0.5pF per mm of electrode length [11]. There exist a trade of between the sensitivity of the MZM (V_π) and its bandwidth. For larger bandwidth the length of the MZM should be

small which according to (2.8) means large V_π. When the period of maximum modulation frequency is high enough compared to the optical transit time, lumped element electrodes are less effective because the modulation voltage is not constant during the optical transit time. Travelling wave electrodes are used under such condition. Travelling wave electrodes are designed such that the RF propagation delay along the travelling wave electrode matches the optical propagation velocity in the waveguide. This is referred to as the velocity matched condition. Travelling wave electrode MZM can achieve GHz of bandwidth with moderate sensitivity.

The main disadvantage of the MZM is it has a large footprint ($\sim 10^4 \mu m^2$) and poor power efficiency but it is less sensitive to wavelength and has less mismatch due to fabrication because of the large footprint.

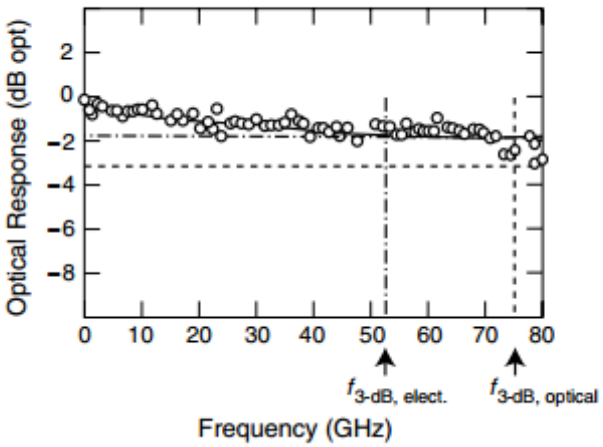

Figure 2.9: Frequency response of a MZM. Reprinted from[20]

2.1.2 Photodetector (PD)

The output of the optical modulation is an intensity modulated optical wave. To recover the electrical signal from the optical carrier requires the use of a photodetector. A photodetector (PD) is a device that performs electrical to optical conversion. The current generated by a PD from an incident light is given as [9]:

$$I = P \cdot R \tag{2.14}$$

where P is optical power of incident light, I is the current and R is the responsivity of the PD. The responsivity of the PD is the amount of photocurrent produced per watt of input optical power[21] .The responsivity of a PD is also given as [9]:

$$R = \eta \cdot \frac{\lambda q}{hc} \tag{2.15}$$

where h is the Planck constant, c is the speed of light in a vacuum, λ is the wavelength, η is the quantum efficiency and q is the charge of an electron.

The most common PD is the p-i-n photodetector or photodiode. A p-i-n PD has an intrinsic (undoped or lightly doped) semiconductor material sandwich between a p and n doped material. The p and n are reversed bias so that an electric drift field is generated in the intrinsic material. When light falls on the intrinsic layer, the photons create electron-hole pairs which become separated by the electric drift field. As a result photonic current flows through the terminals. The thickness of the intrinsic layer (Fig.2.3 (a)) poses a trade of between speed and the percentage of photons that create electron-hole pairs (quantum efficiency). Thicker i-layer means high quantum efficiency but less speed and vice versa. Modern waveguide p-i-n PD (Fig.2.3 (b)) breaks this trade off by illuminating the i-layer horizontally from the side and the electric field is orthogonally formed. This approach allows the quantum efficiency to be controlled by the horizontal dimension whiles the speed is controlled by the vertical dimension. High speed p-i-n PD mostly uses this approach. Recent years have seen the development of other device structures that have a potential for high bandwidth and responsivity such as metal-semiconductor -metal (MSM) diodes [21].

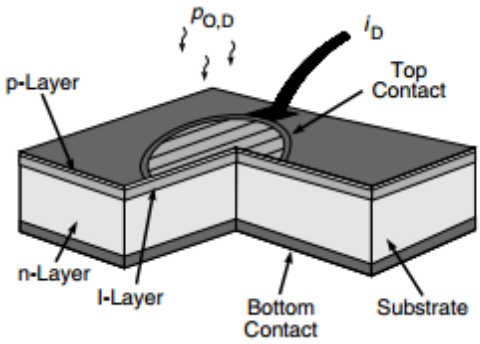

(a)*Reprinted from*[11]

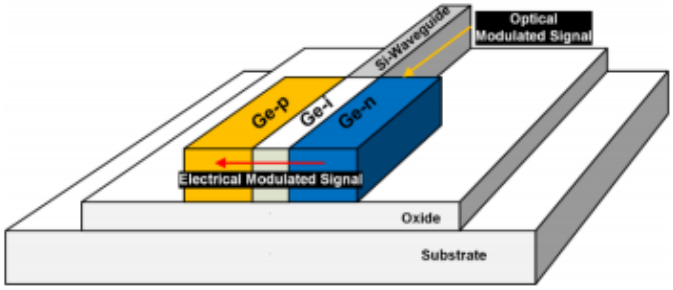

(b)*Reprinted from*[22]

Figure 2.10: Photodetectors (a) P-i-n (b) Waveguide p-i-n

2.2 Mach-Zehnder Modulator Non-linearities

The MZM transfer function given in (2.6) is non-linear so generates significant harmonics and intermodulation products especially as the electrical signal applied to it gets larger. The nonlinearity generated from the MZM is at least ideally independent of the frequency [23].

Firstly look at the amplitude of the harmonics when a single tone RF signal (V_{RF}) is applied to the RF terminal of the MZM. Assuming the RF signal applied is:

$$V_{RF} = Asin(\omega t + \theta) \tag{2.16}$$

Inserting (2.16) into (2.6) and with further manipulations generates:

$$P_{m,out} = \frac{T_{FF}P_{in}}{2}\left(1 + cos\varphi_b \cos\left(\frac{\pi A}{V_\pi} sin(\omega t + \theta)\right) - sin\varphi_b sin\left(\frac{\pi A}{V_\pi} sin(\omega t + \theta)\right)\right) \tag{2.17}$$

Using Bessel function trigonometric identities given by [24] in (2.16) gives:

$$P_{m,out} = \frac{T_{FF}P_{in}}{2}\left(1 + cos\varphi_b J_0\left(\frac{\pi A}{V_\pi}\right) + 2\sum_{l=1}^{\infty} J_{2l}\left(\frac{\pi A}{V_\pi}\right) cos\varphi_b \, cos(2l(\omega t + \theta)) - 2\sum_{l=1}^{\infty} J_{2l-1}\left(\frac{\pi A}{V_\pi}\right) sin\varphi_b \, sin((2l-1)(\omega t + \theta))\right) \tag{2.18}$$

From (2.18) we can observe that when $\varphi_b = \frac{\pi}{2}$, the amplitude of all the even order terms will go to zero. Likewise, when $\varphi_b = 0 \; or \; \pi$ the amplitude of the odd order component will go to zero and only the even order terms will exist. The harmonics are not very critical when the MZM is used in a system that operates over less than an octave bandwidth as they can be removed by filtering.

A very important non-linearity consideration of a MZM especially when it is used in an RF application is the intermodulation products generated when a two tone signal is applied to the RF port of the MZM. The intermodulation products generated especially the third-order intermodulation can be really close to the desired signal frequency depending on the frequency of the two tones and as such it is impossible to filter out. It therefore has the potential of corrupting the desired signal. Assuming two tone input RF signal of the same amplitude $V_{RF,1} = Asin(\omega_1 t + \theta_1)$ and $V_{RF,2} = Asin(\omega_2 t + \theta_2)$ are applied to the RF terminal of the MZM modulator. All the spectral component at the output of the MZM is given by [25] as:

$$
\begin{aligned}
P_{m,out} = \frac{T_{FF}P_{in}}{2}\Bigg(& 1 + {J_0}^2(z)cos\varphi_b \\
& + 2cos\varphi_b \sum_{n=0}^{+\infty}\sum_{m=0}^{+\infty} (\pm 1)^n J_n(z) J_m(z) \cos\big(n(\omega_1 t + \theta_1) \\
& \pm m(\omega_2 t + \theta_2)\big) \\
& - 2sin\varphi_b \sum_{n=0}^{+\infty}\sum_{m=0}^{+\infty} (\pm 1)^{n+1} J_n(z) J_m(z) \sin(n(\omega_1 t + \theta_1) \\
& \pm m(\omega_2 t + \theta_2)) \Bigg)
\end{aligned}
\tag{2.19}
$$

where J_n represent the first kind of Bessel of the nth other and $z = \frac{\pi A}{V_\pi}$. The first double summation has the condition that $n + m \geq 2$ $(even)$ and the other $n + m \geq 1$ (odd). The amplitude of the fundamental component can be express by [25]:

$$
-2 \cdot \frac{T_{FF}P_{in}}{2} J_1(z) J_0(z) sin\varphi_b \tag{2.20}
$$

The amplitude of the second-order intermodulation products is also given as [25]:

$$\pm 2 \cdot \frac{T_{FF} P_{in}}{2} {J_1}^2(z) cos\varphi_b \tag{2.21}$$

Finally, the third-order intermodulation products can be expressed as [25]:

$$-2 \cdot \frac{T_{FF} P_{in}}{2} J_2(z) J_1(z) sin\varphi_b \tag{2.22}$$

From the above equations it can be concluded that the amplitude of the second order intermodulation products reduces to zero when $\varphi_b = \frac{\pi}{2}$. It can also be seen that the relative third order intermodulation which is define as the ratio between the amplitude of the third order intermodulation and the amplitude of the fundamental does not change with φ_b.

2.3 Mach-Zehnder Modulator Linearization

Several techniques for linearization of the MZM has been reported in literature. There are two main approaches: optical linearization solution and electrical linearization solution.

2.3.1 Optical Solution

The optical linearization solution entails using the MZM in different configurations to make it more linear.

2.3.1.1 Series MZM

[26]–[28]uses a structure which consist of two standard (MZM) connected in series. The RF input power is split between the two modulators such that the second MZM has modulation depth r compared to the first MZM.

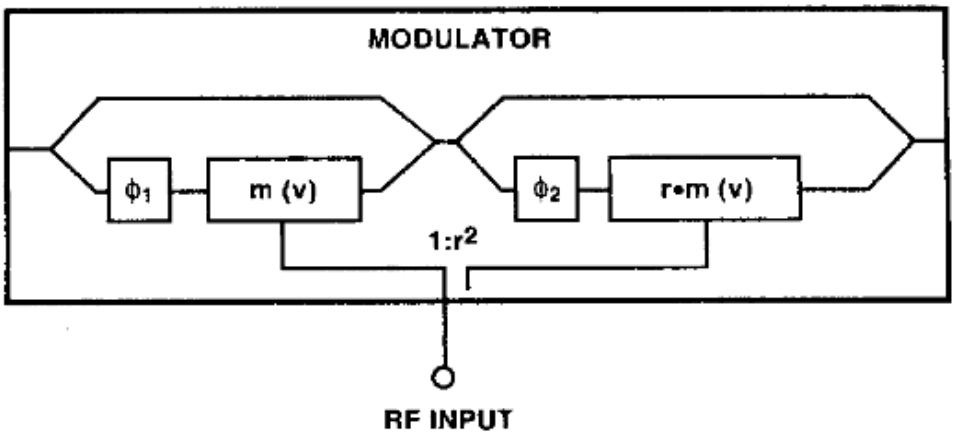

Figure 2.11: Series Mach-Zehnder modulator. Reprinted from[28]

To reduce the third order intermodulation of the series MZM structure requires the reduction of the cubic terms of the transfer function. For two MZM's in series, the cubic term is generated from the cubic term of the individual MZM's and the product of the linear terms of one MZM and the quadratic term of the other. The DC bias of φ_1 *and* φ_2 of the first and second MZM respectively and r are chosen such that the cubic product term cancels the cubic term of the individual MZM while the linear terms from the individual modulators add up. When the cubic nonlinearity cancels out, the linearity of the cascaded structure now becomes limited by the fifth order nonlinearity. If an extremely linear structure is required an additional MZM can be cascaded to cancel the fifth order nonlinearities[29]. The series MZM is a relative simpler approach to reducing the third order intermodulation but it requires a lot of footprint. In addition, there is an optical power penalty generated by this structure because of the extra optical loss generated by the second MZM (3-6dB). This can be reduced to ~0.5dB by integrating both MZMs on the same chip. Another disadvantage of this approach is for the cubic cancellation to work correctly, the electrical signals applied to the two modulators must be in phase that is the electrical signal applied to the second modulator must arrive the same time as the light from the first modulator that was modulated by the same signal. This is difficult to achieve

at higher frequencies where the period of the electrical signal is comparable to the optical transit time

2.3.1.2 Dual Polarization Technique

[30], [31] uses an MZM that support both single TE and TM modes and has unequal electro-optic sensitivity to both. A polarizer is placed between the MZM and the optical source and it is used to adjust the relative amounts of TE and TM input optical power. The total output power is the sum of both modes.

The third order intermodulation of each mode is given as in (2.12). If $z \ll 1$ then it can be approximated as [31]:

$$\frac{-1}{16} T_{FF} P_{in}(z)^3 sin(\varphi_b) + \text{higher-order terms} \tag{2.23}$$

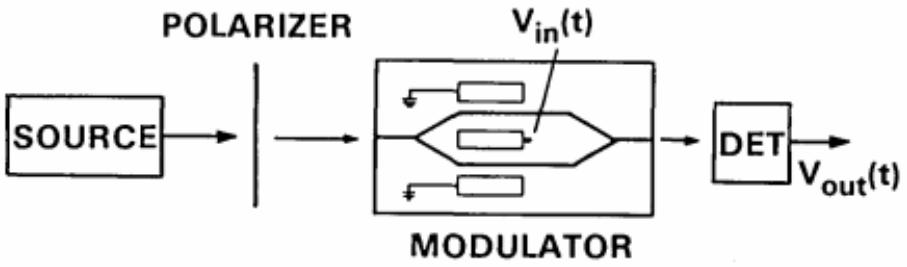

Figure 2.12: MZM with dual polarization. Reprinted from[31]

$$z^{TE} = \gamma z^{TM} \tag{2.24}$$

The dc bias voltage of the both modes and the input polarizer power can be adjusted such that the third order intermodulation from the individual modes cancel each other when they two modes sum up to form the total output. [31] finds the

optimum condition for the cancellation of the third order intermodulation terms to be:

$$\varphi_b{}^{TM} = -\frac{\pi}{2} \quad and \ \varphi_b{}^{TE} = \frac{\pi}{2} \tag{2.25}$$

$$P_{in}{}^{TM} = \gamma^3 P_{in}{}^{TE} \tag{2.26}$$

The disadvantage of this approach is that most of the input power is now TM polarized which results in a reduction in the sensitivity at the fundamental frequency by approximately a factor of γ compared with using only TE mode. $\gamma \sim 3$ in lithium niobate modulators [31].The reduction in the sensitivity translates to an optical power penalty.

2.3.1.3 Dual Parallel MZM

[32]–[34] uses two MZM connected in parallel fed with different optical power. The incoming optical power is split between the two MZMs. The MZMs are driven to different modulation depths. The RF power and optical power are split in such a manner that the MZM with less RF signal carriers the maximum portion of the optical power and vice versa. The two optical outputs can be combined optically using a waveguide or incoherently as shown in Fig.2.13 by combining the electrical outputs of two separate detectors. The MZM driven to less modulation depth generates less distortion whiles the MZM driven to a relatively higher depth generates more distortion. The bias points of the MZMs are chosen such that the modulations are out of phase. If proper splitting ratio of both the RF and optical power is chosen, the distortion terms cancel out while the main signal does not cancel out completely. The proper splitting ratio can be determine using the same idea from [31] as the two approaches are similar. The disadvantages of the dual parallel MZM are the optical

power penalty generated, large footprint and it requires two drivers to drive the modulator which translate to increase in electrical power.

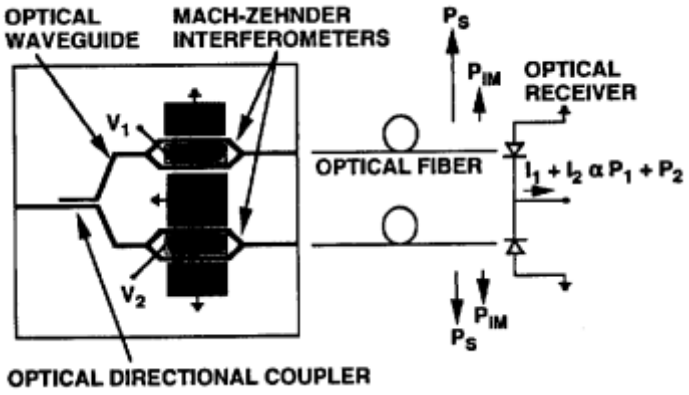

Figure 2.13: Dual parallel MZM. Reprinted from[32]

2.3.1.4 Ultra-linear External Modulator

[35] proposed a new modification to the MZM to increase its linearity. The structure is similar to a typical MZM but with a phase modulator and a ring resonator of coupling coefficient γ connected in series on one arm of the arm. The RF signal is split in the ratio F: 1-F and then applied to the electrode of the phase modulator and the ring resonator modulator respectively. The structure is biased at the quadrature point so that the even order nonlinearities will ideally be zero. The ring resonator modulator is not operated at resonance. The ring resonator provides the necessary phase correction without affecting the magnitude. An optimum value is set for the RF signal split ratio and the ring resonator coefficient that results in the cancellation of the third order terms and even possibly the fifth order terms in the Bessel expansion of the entire system transfer function thus rendering the system linear .The advantages of this structure are it requires relatively less footprint and relatively lower loss. The disadvantage is it requires an extra component to split the RF signal

to the appropriate ratio. The RF splitters are problematic especially as the frequency of operations becomes larger.

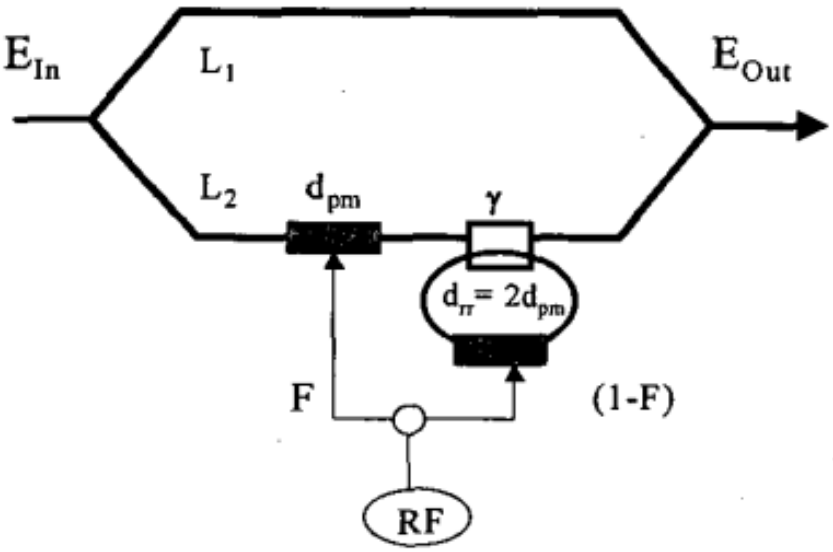

Figure 2.14: An ultra-linear MZM. Reprinted from[35]

2.3.1.5 Ring Assisted Mach-Zehnder Interferometer (RAMZI)

[36], [37] proposed a modulator which consist of a MZI with one or two ring resonators on both arms. The RF signal is fed to the electrodes of the ring resonators in a push-pull fashion. The modulator is operated at the quadrature point which means a quarter delay period exist between the two arms. The effective optical length of each ring resonator is chosen such that it is an odd number multiple of the half operating wavelength in order for them to operate in the off resonate state. The output intensity of the RAMZI as a function of the refractive index change inside the ring resonator is given in [36] as:

$$I_{out} = \frac{1}{2} I_{in}(1 + \sin(\phi_A(\Delta n) - \phi_B(\Delta n)) \qquad (2.27)$$

$$I_{out} = \frac{1}{2} I_{in} \left(1 + (\phi_A(\Delta n) - \phi_B(\Delta n) - \frac{1}{6}(\phi_A(\Delta n) - \phi_B(\Delta n))^3 + \cdots\right) \tag{2.28}$$

where ϕ_A and ϕ_B are the phase delay introduced by the ring resonator in the upper and lower arm respectively. To make the structure more linear requires the cancellation of the cubic term. The condition that this occurs is given in [36] as:

$$\left(\left(\frac{1-\rho_A}{1+\rho_A}\right) C_A - \left(\frac{1-\rho_B}{1+\rho_B}\right) C_B\right)^3 = 2\left(\frac{(1-\rho_A)}{(1+\rho_A)^3} {C_A}^3 - \frac{(1-\rho_A)}{(1+\rho_A)^3} {C_A}^3\right) \tag{2.29}$$

where C_A and C_B are the circumference of the upper and lower ring resonator respectively and ρ_A and ρ_B are the through-path ratio of the upper and lower ring resonator. A good feature of the RAMZI is that the ring resonator should operate in an off resonant state. Because of this, it can tolerate ring loss and other imperfection which occur in the ring during fabrication. In addition, since the rings are driven in a push-pull fashion they can be driven by a single fully differential driver which reduces the complexity of the driver circuit. The main disadvantage of the RAMZI is the tradeoff between the modulation efficiency and the bandwidth. For good modulation index efficiency requires the use of rings with long length. As travelling wave driving electrode cannot be used in the ring arrangement, the bandwidth is limited severely when rings with long length are used [36]. Using GaAs–GaAls grown on a (111) substrate would help break the tradeoff but such an approach is expensive. The RAMZI in general has a bandwidth almost half of the standard MZI modulator [36].

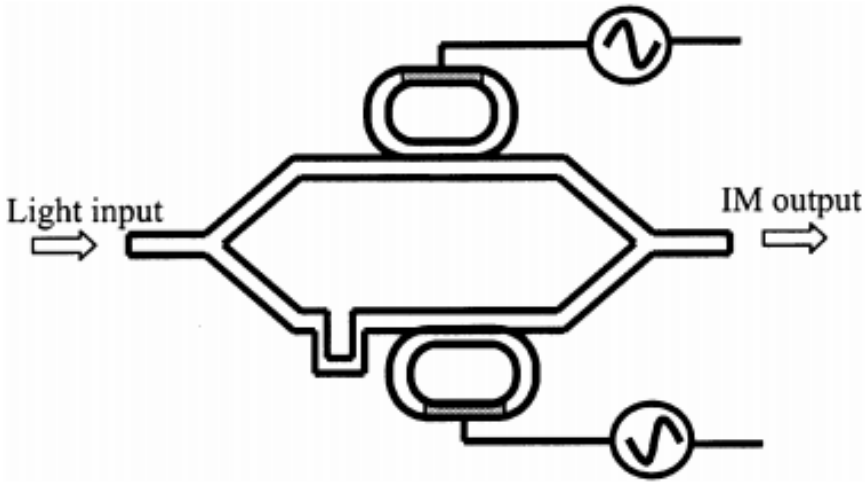

Figure 2.15: RAMZI.Reprinted from[36]

2.3.1.6 Dual Wavelength Technique

[38] as shown in Fig.2.16 uses a commercially available MZM with a single dc bias electrode and a single travelling wave RF electrode. The MZM is used to modulate two wavelengths of light simultaneously. At the output of the MZM is a wavelength-division multiplexer (WDM) that routes the two modulated wavelength to two separate detectors. The output of the detectors are combined in an RF hybrid coupler. Linearization of the MZM is achieved by choosing a dc-bias point such that the even order distortion at both wavelengths is zero and setting the ratio of the current of the detectors to the cube of the ratio of the switching voltages of the MZM at the two wavelengths. The advantages are the linearization can be done using commercially available components and an electronic circuit can be used to adaptively control the detector current ratio in unpredictable environmental conditions. The main disadvantage are: it requires a really high dc bias voltage (~+18V) for the even order distortion in both wavelengths to be close to zero and it requires two laser sources and several other component which makes the approach expensive .

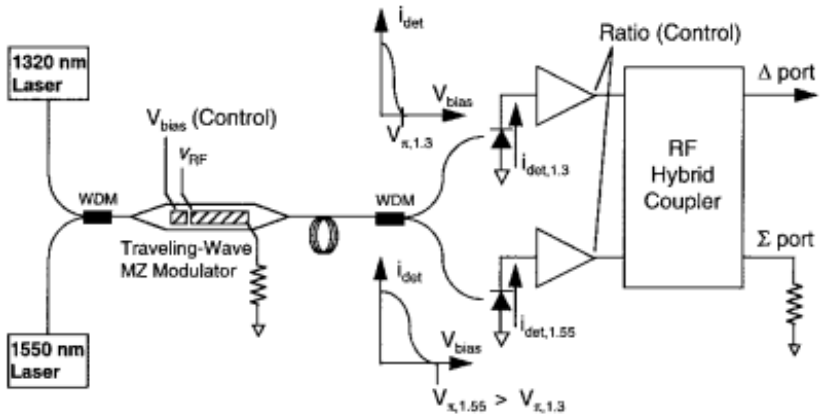

Figure 2.16: Dual wavelength technique. Reprinted from[38]

2.3.2 Electrical Solution

The electrical solution entails aiding the MZM with electrical circuits so that the overall system will be more linear. There are two main approaches reported in literature: feedforward and predistortion linearization.

2.3.2.1 Feedforward Linearization

Another approach to dealing with the intermodulation generated as a result of the non-linear transfer function of the MZM is using feedforward [39], [40] . The feedforward linearization is a two-loop architecture. The RF signal is used to modulate the MZM and part of the output is coupled out and converted back to an electrical signal using and optical to electrical converter (O/E). An example of an O/E is a photodetector. Part of the input RF signal is passed through an amplitude and phase adjustment block. The output of the O/E block is added to the output of the amplitude and phase adjustment block. When the output of the amplitude and phase adjustment block is set to the right amplitude and right phase (anti-phase to the output of the O/E block), the summation produces only the intermodulation term. The output of the summation is also passed through an amplitude and phase

adjustment block and then modulates an optical carrier using another MZM. The output of the MZM is coupled back to the output of the main MZM. With the proper phase and amplitude settings, the signal coupled back will ideally cancel the intermodulation terms generated by the main MZM and the resulting amplitude will be perfectly linear. The feedforward linearization is attractive because prior knowledge of the input is not required and the same architecture will not only work for an MZM but will also easily work for any of the optical modulators mentioned in the previous section with very little or no change at all. The main disadvantages is: it requires two lasers and several other components. This makes the feedforward linearization complex and expensive. In addition, for proper performance the circuits in the feedforward paths have stringent linearity requirements and the approach has stronger sensitivity to amplitude and phase balancing.

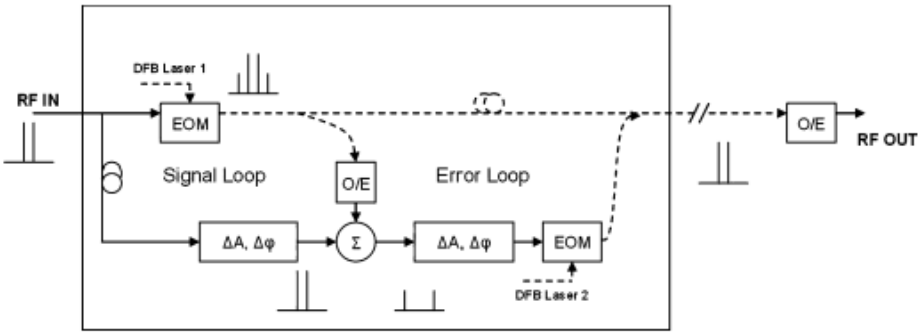

Figure 2.17: Feedforward linearization. Reprinted from[39]

2.3.2.2 Predistortion Linearization

The predistortion is the more common of the two reported in literature because it is relatively less complex, cheaper to implement and it requires less optical components compared to the feedforward linearization. In predistortion linearization the input RF signal is preconditioned such that when applied to the MZM, makes the output of the MZM more linear. The general idea behind the

predistortion is that a transfer function exist that can be placed between the RF signal and the MZM that will make the overall system linear. Ideally the optimum transfer function is an arcsine as the MZM has a cosine transfer characteristics. Traditionally arcsine circuits have been realized using diodes and bipolar transistors. They take advantage of the exponential transfer characteristics of these devices[41]–[43]. The use of bipolar transistors are expensive and bars system integration. Complementary metal-oxide semiconductor (CMOS) technology circuit is more attractive but it is very hard to build circuits to achieve ideal arcsine transfer function.

[44] leverages the square characteristics of long channel cmos transistors to build a circuit with an arcsine characteristics. The response of the circuit is a polynomial whose coefficients matches the Taylor series expansion of an arcsine up to the fifth order. As fifth order polynomial Taylor series expansion of an arcsine is just an approximation of an arcsine, it has a limitation to the amount of linearization that it can be achieved especially when the input signal gets larger. Despite the fact that it is not an ideal arcsine implementation, it was able to achieve significant linearization up to about 49.6% modulation index. The core of the arcsine circuit is shown in Fig.2.18. The output current of a clipping transconductance amplifier (inner pair) is subtracted from that of a linear amplifier (outer pair) and the resulting differential current can be expressed in terms of the input differential voltage as a polynomial. By choosing the appropriate transistor sizes, the coefficients of the polynomial up to the fifth order will be able to match that of the Taylor series expansion of an arcsine. A PMOS current mirror is used to combine two arcsine circuit which is followed by a transimpedance amplifier (TIA) to convert the current to voltage (Fig.2.19). The output of the TIA is the followed by a buffer which drives the PA that drives the MZM.

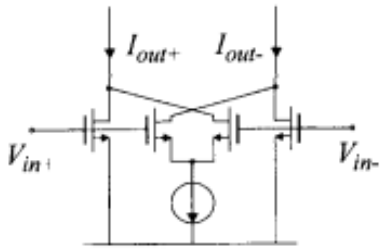

Figure 2.18: The arcsine core. Reprinted from[44]

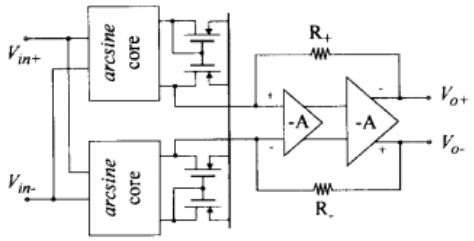

Figure 2.19: Fully balanced arcsine circuit. Reprinted from[44]

[45] implemented a third-order polynomial (Fig.2.20). The implementation is done having three paths: main path, second-order path and third-order path in parallel. The output of the paths are summed together to generate the third-order polynomial. The second-order path and the third-order path each has a variable gain amplifier (VGA) that can be adjusted independently. This allows the third-order polynomial coefficients to be changed independently. The square function is achieved by connecting the drain and source of two NMOS transistors together. The joined drains are connected through a resistor to the supply. The cubic function is generated using the same circuit shown in Fig.2.18 but in this case the sizing of the transistors are done such that the differential current out is directly proportional to the cube of the differential input voltage. A time delay is placed in the main path such that the main path matches in phase with the second-order and third-order paths. The predistortion circuit implemented is versatile in the sense that it can be

used to linearize several other non-linear optical devices like DFB laser etc. This feature makes it attractive. The phase adjustment block which is implemented using a fifth-order polyphase filter helps it to achieve this versatility. With the phase adjustment block, it is able to linearize for both static nonlinearity that is nonlinearity common to MZM and dynamic nonlinearity (frequency dependent nonlinearities). The polyphase filter is made up of resistors and capacitors so consumes a lot of area and the predistortion circuit only implements third-order polynomial so it is not able to achieve good linearization as the signal amplitudes get bigger. These are the main drawbacks of the implementation.

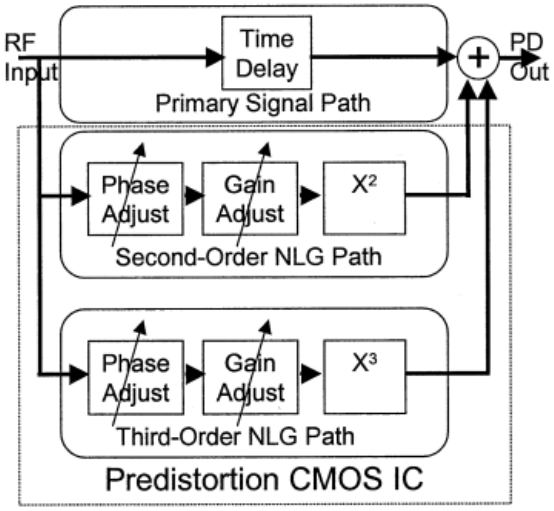

Figure 2.20: Third-order predistortion block diagram. Reprinted from[45]

3 PROPOSED SOLUTION

3.1 Concept of Proposed Solution

The proposed predistortion is a fifth-order predistortion. Like [45] the polynomials are chosen not to depict the Taylor series polynomial of an arcsine but rather to force the intermodulation products to zero. To highlight the advantage of the fifth-order polynomial implemented compared to the third-order polynomial implemented in [45], we will first look at the third-order predistortion. The third-order predistortion is shown in Fig.3.1. Assuming the MZM is perfectly biased at the quadrature point, then there is no need for the squaring path in the third-order predistortion thus the omission. Also for ease of explanation, the MZM transfer function from the RF input to the optical output is approximated as a polynomial. When two tone RF signal is applied to the predistortion, it goes through the linear path and the cubing path. The sum of signals from the linear path and the cubing path of the predistortion enters the MZM and it travels through the linear path, cubing path and raised-to-the fifth path. The output of the linear path of the MZM can be decomposed into two: output due to the linear path of the predistortion and output due to the cubing path of the predistortion. The output of the cubing and raised-to-the fifth path of the MZM can also be decomposed into two: output due to the signal through the linear path of the predistortion and output due to a product of the linear path and cubing path of the predistortion. The final output of the MZM is the sum of the various decompositions. The decompositions contain both third-order and fifth-order intermodulation products. The third-order predistortion has only one control variable so can only be optimized for either a very low (ideally zero) third-order intermodulation products or a very low (ideally zero) fifth-order intermodulation products as depicted in Fig.3.1. This limit the amount of third-order and fifth-order intermodulation products suppression that the third-order predistortion can achieve as the signal amplitude of the two tones increases. It can be observed that if

an extra control variable existed then optimization could be done for both third-order and fifth-order intermodulation product suppression.

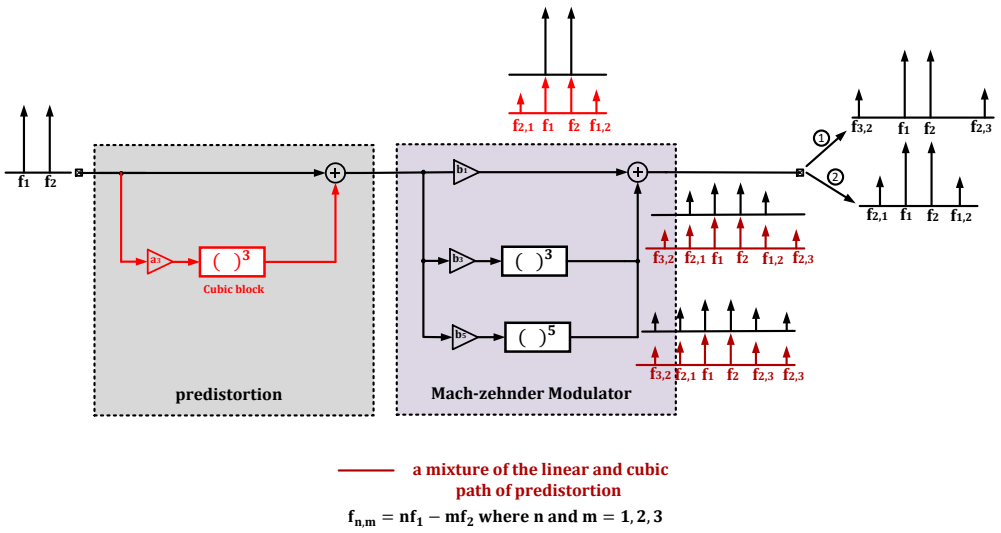

Figure 3.1: Operation of third-order predistortion

The fifth-order predistortion (Fig.3.2) has an additional parallel path that performs a raised-to-fifth function. When two tone RF signal is applied to the predistortion, it goes through the linear path, the cubing path and the raised-to-the fifth path. The sum of signals from the linear path, the cubing path and raised-to-the fifth of the predistortion enters the MZM and it travels through the linear path, cubing path and raised-to-the fifth path. The output of the linear path of the MZM can now be decomposed into three: output due to the linear path of the predistortion, output due to the cubing path of the predistortion and output due to the raised-to-the fifth path of the predistortion. The output of the cubing and raised-to-the fifth path of the MZM can also be decomposed into three: output due to the signal through the linear path of the predistortion, output due to a product of the linear path and cubing path of the predistortion and output due to a product of the linear path and raised-to-the fifth path of the predistortion. The final output of the MZM is the sum of the various

decompositions. The introduction of the raised-to-the fifth path gives an extra control variable such that both the third-order and fifth-order intermodulation products can be minimized (ideally zero).

As the two tone signal goes through the cubic and raised-to-the fifth path of the MZM, the finite delay of the blocks introduce a delay/phase shift (Fig.3.3) to the signal at their output. The signal through the linear path of the predistortion has no delay as it goes through no element. The delay mismatch causes the intermodulation products to be out of phase such that even if the right coefficients are set for the predistortion polynomial, the intermodulation products do not cancel out at the output of MZM (Fig.3.3). This is corrected by placing the time delay in the linear path of the MZM so that delay of the paths can be matched. With the delay matched the coefficients can be chosen such that the intermodulation products cancel out at the output of the MZM (Fig.3.4).

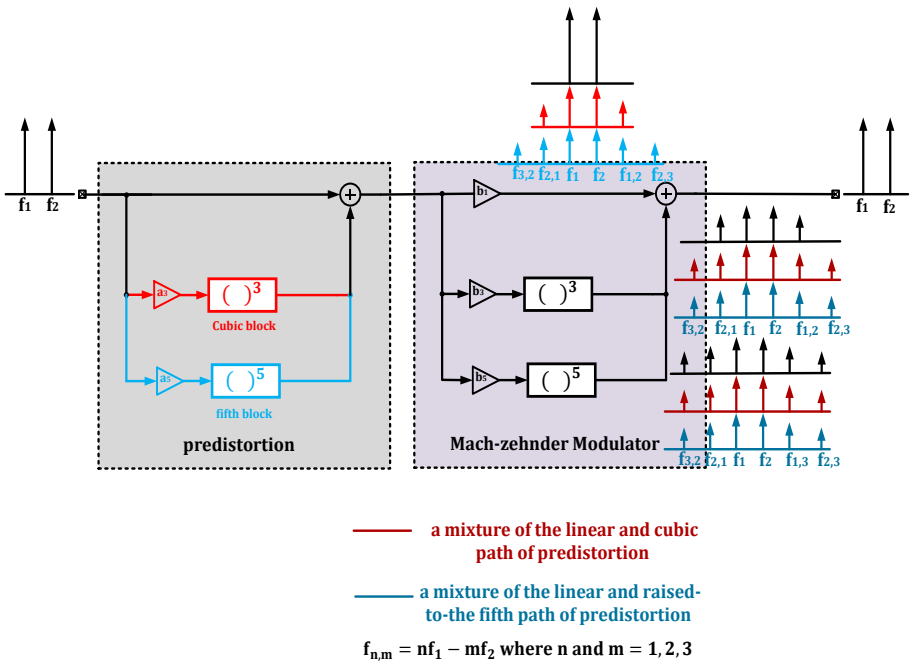

Figure 3.2: Operation of the fifth-order predistortion

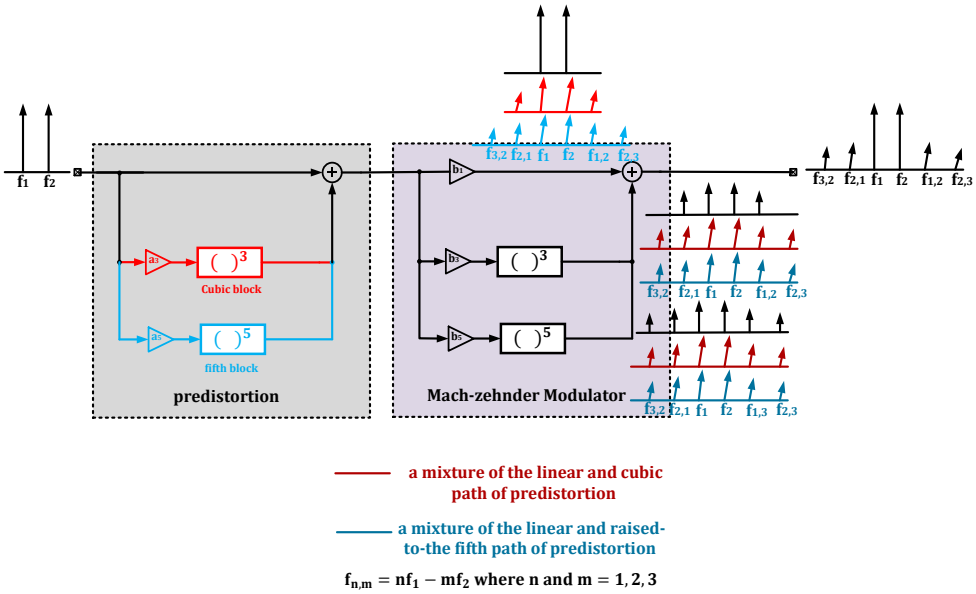

Figure 3.3: Effects of finite delay of predistortion elements

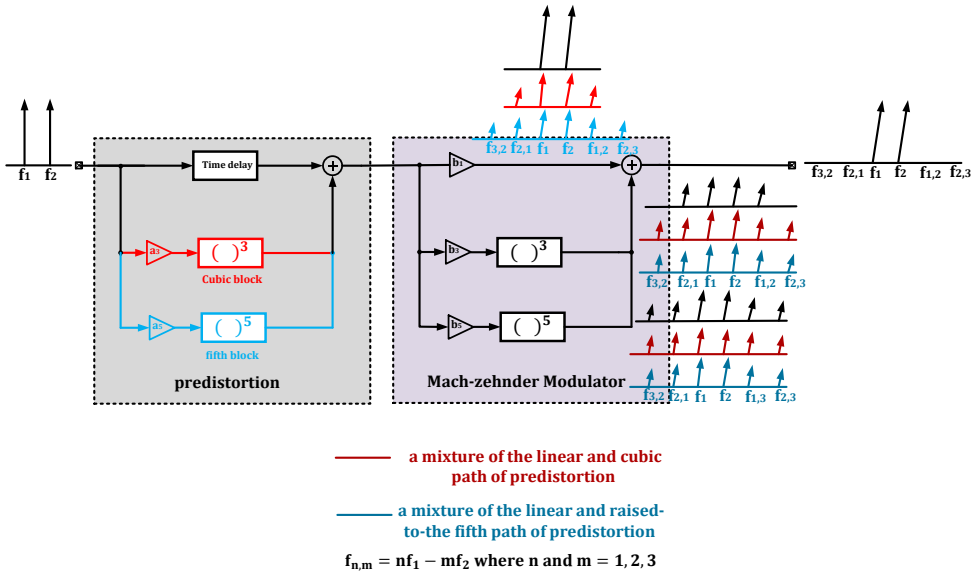

Figure 3.4: Compensation of finite delay

Fig.3.5 and Fig.3.6 shows the comparison between the proposed solution and the two existing predistortion approaches. The results were obtained by constructing ideal models for the various predistortion techniques and using the ideal MZM

transfer function. The ideal predistortion models contain perfect cubing and raised-to-the fifth paths with no delay. It can be see that the at low modulation index, the proposed solution performs similarly to the fifth-order arcsine approximation predistortion but as the modulation index increases proposed solution achieved (~10-16dB) better performance than the fifth-order arcsine approximation predistortion and the third-order predistortion with IM5 optimized. At really high modulation index (< 58%) the proposed solution achieves ~5dB better. Although the third-order predistortion with IM3 optimized has a better IM3 than the proposed solution, the IM5 of the third-order predistortion with IM3 optimized is less than the IM3 so it's limited by IM5 and not IM3. If the IM5 is compared to the IM3 of the proposed solution it is seen that the proposed solution ~10-16dB better at moderately high modulation index (43% < and <53%).

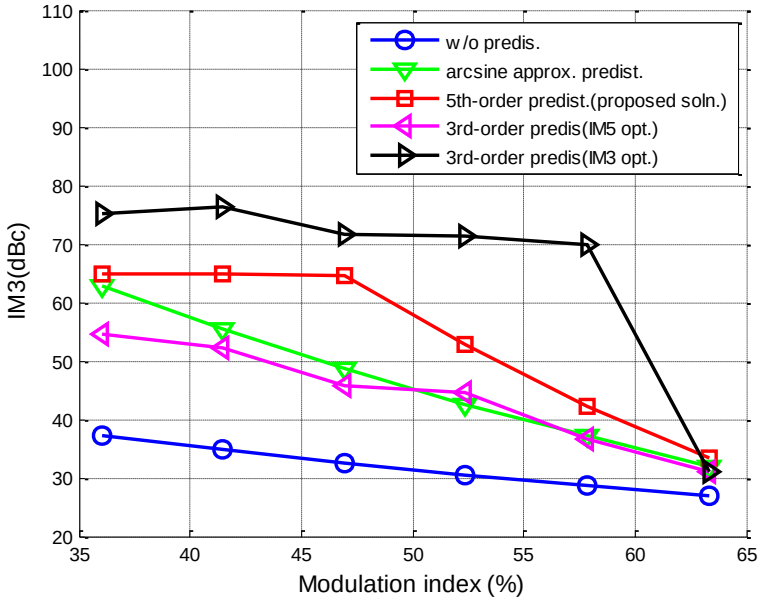

Figure 3.5: IM3 vs modulation index for different predistortion

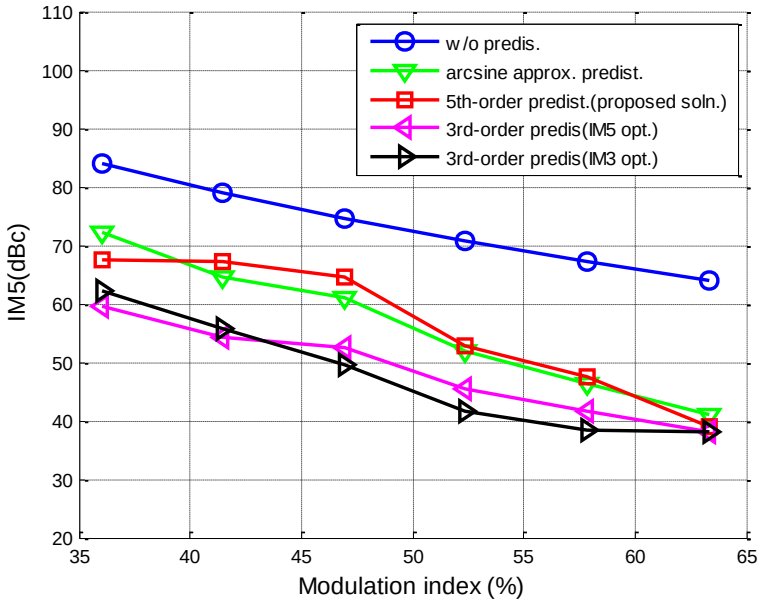

Figure 3.6: IM5 vs modulation depth for different predistortion

3.2 Circuit Implementation

A fifth-order predistortion system block diagram is shown in Fig.3.7. It has three parallel paths: main path, cubic path and the raised to the fifth path. The outputs of the paths are summed together using a current mode summer whose outputs drive a buffer which then drives an external power amplifier. The cubic and raised-to-the -fifth paths each have a variable gain block preceding it which generates the coefficients of the fifth-order polynomial. This arrangement is done to increase the gain tunability of the variable gain blocks. For the main path to add in phase with the cubic and raised-to-the-fifth block, an analog gm-c time delay block is added to the main path. The gm-c time delay block is made tunable to account for process and temperature variation. The gain tunability is achieved through variation of the capacitance .

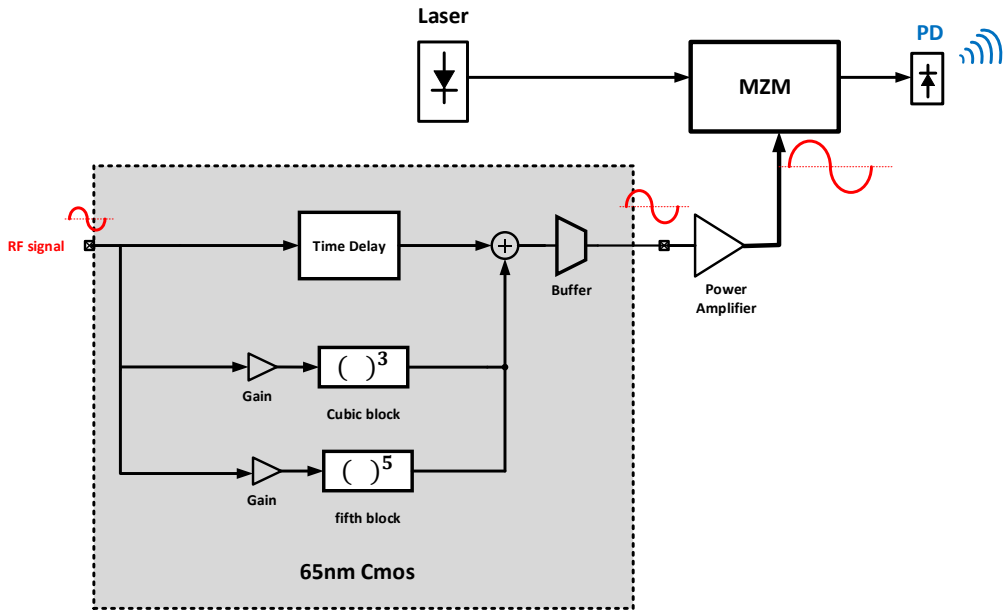

Figure 3.7: System block diagram of fifth-order predistortion

3.2.1 Analog Time Delay

An ideal time delay block has transfer function given as $H(s) = e^{-s\tau}$. The phase is linearly related to the frequency.Implementation of the ideal delay block is not possible.Several IC compatible circuits to approximate a time delay exist in literature, examples are: Transmission lines[46], [47], LC delay lines[48], switched capacitor delay circuits[49] and gm-C all-pass filters[50]. At low-GHz frequecies(~2GHz) which is the operation of the fifth-order predistortion, transmission lines and LC delay lines in CMOS are impractical due to the low quality factor and size of inductors, and the loss of the transmission lines [50]. The switch capacitor on the other hand are too slow for low-GHz applications. A pseudo-differential version of the analog time delay of [50] is implemented because of its minimum area requirement and simplicity(Fig.3.8). A pseudo differential version is implemented instead of a fully differential version in order to be able to have enough headroom to design M1 to have high overdrive without going into the triode region. This is done to achieve good linearity for the delay block which is important for the

proper performance of the predistortion circuitry.The circuit transfer function implements a first-order allpass filter . The transfer function of a first-order allpass filter is given as :

$$H(s) = \frac{1 - s\left(\frac{\tau}{2}\right)}{1 + s\left(\frac{\tau}{2}\right)} \tag{3.1}$$

It can be rewritten as a combination of a lowpass and a DC gain of one as shown below:

$$H(s) = \frac{2}{1 + s\left(\frac{\tau}{2}\right)} - 1 \tag{3.2}$$

(3.2) represents the basis of the implementation of the all-pass filter shown in Fig.3.6. The lowpass filter is implemented through M1, M4, M5 and M3 and the DC gain of -1 is implemented through M2 and M3. The ideal transfer function of Fig.3.9 is given as:

$$H(s) = \frac{1 - s\frac{C}{gm_4}}{1 + s\frac{C}{gm_4}} \tag{3.3}$$

where the delay is given as:

$$\tau \approx \frac{2C}{gm_4} \; and \; C = B_0C_0 + B_1C_1 + B_2C_2 \; where \; B_{0,1,2} \; is \; either \; 0 \; or \; 1 \tag{3.4}$$

The delay is varied by varying C by setting $B_{0,1,2}$ *to either* 0 *or* 1. To get constant delay over a wider frequency band places a limitation on the amount of delay that can be implemented[51]. To generate a large delay over a wider frequency band

requires cascading a number of the all-pass filter shown in Fig.3.8. In this work two of the all-pass filters were cascaded to generate the amount of delay required.

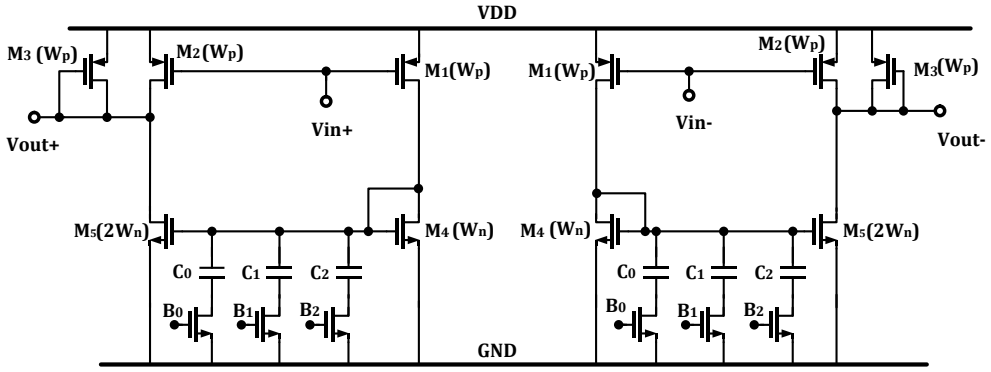

Figure 3.8: All-pass delay cell

Considering the non-idealities of the delay cell as shown in Fig.3.9, the transfer function is given by [50] as:

$$H(s) = \frac{1 - \frac{2}{gm_n}\left(gds_n + gds_p\right)}{1 + \frac{2}{gm_p}\left(gds_n + gds_p\right)} \cdot \frac{1 - \frac{sC}{gm_n}}{1 + \frac{sC}{gm_n}} \cdot \frac{1}{1 + \frac{sC_L}{gm_p}} \tag{3.5}$$

$$For\ gm_n \gg 2\left(gds_n + gds_p\right) \tag{3.6}$$

$$and\ \ gm_p \gg 2\left(gds_n + gds_p\right) \tag{3.7}$$

where gm_p and gds_p are the transconductance and output conductance of M_1, M_2 and M_3 in saturation, gm_n and gds_n are those of M_4 and $2gm_n$ and $2gds_n$ of M_5. C now includes the parasitic capacitances $C_{gs,M4}, C_{gs,M5}, C_{db,M4}$. C_L is sum of the next stage input capacitance$\left(C_{gs,M1} + C_{gs,M2}\right)$ and $C_{gs,M3}\ and\ C_{db,M3}$.It can be seen from (3.5) that the DC gain is not unity and there is an additional pole. This pole can be viewed as one-third of the unity current gain frequency (f_t) of the CMOS process. Which will

be around tenths of GHz in the TSMC 65nm GP process so the effect of the pole can be neglected for the operating frequency of the implemented delay cell. The non-unity DC gain is compensated by sizing M_5 as $2(1+\alpha)W_n$ and M_2 as $(1+\alpha)W_p$ which will increase the DC gain by $(1+\alpha)$. This will cause the output common mode to move down. For higher α values a current source PMOS sized as αWp can be connected in parallel to M_2 and M_3. This will steer some of the current from M_3 and reduce the reduction of the output common mode.Fig.3.10 shows the response of the implemented delay. It has a group delay variation of ~6ps and gain variation of 0.5dB over 500MHz bandwidth. This is enough for the predistortion system implemented.

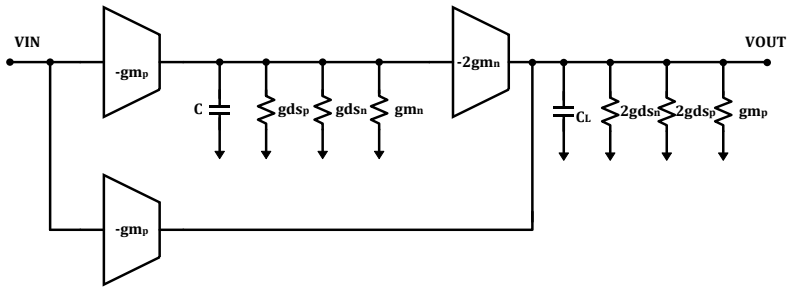

Figure 3.9: Block diagram of delay cell with non-idealities

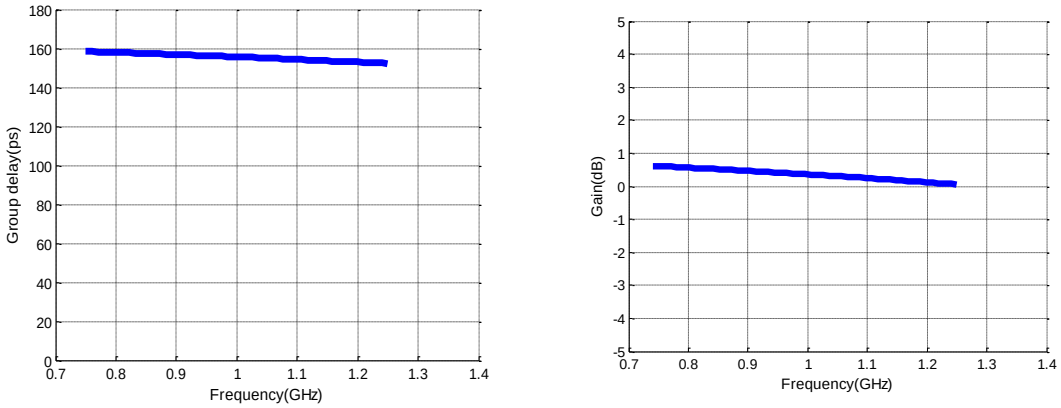

(a) (b)

Figure 3.10: (a) Group delay (b) Gain

3.2.2 Summer

The summer consist of three differential pairs with their outputs connected to a resistor, Fig.3.11. The differential pairs convert the signal voltages of the three paths to current and sum them on a resistor. The signal from the main path is large so in order not to distort it the differential pair of the main path is source degenerated. The output voltage of the summer is given in (3.8).

$$Vout(s) \approx \left(\frac{\left(\frac{gm_{1,2}}{1 + gm_{1,2}R_s} \right) V_{in}(s) + gm_{3,4}(V_{in}(s))^3 + gm_{5,6}(V_{in}(s))^5}{gds_{1,2} + gds_{3,4} + gds_{4,5} + g_D} \right) \Bigg/ \left(1 + \frac{sC_{par}}{gds_{1,2} + gds_{3,4} + gds_{4,5} + g_D} \right) \tag{3.8}$$

For the predistortion circuit (Fig.3.7) performance not degraded requires that the individual circuits block have good linearity. For simplicity we will assume the nonlinearities generated from the differential pairs are independent of each other. Firstly, we will look at the nonlinearities generated from the non-degenerated pair ($M_{3,4}$ and $M_{5,6}$). The differential current generated by the differential pairs is given as:

$$Vout_{diff} \approx \left(\frac{1}{2} \mu_n C_{ox} \frac{W}{L} V_{in} \sqrt{\frac{4I_{ss}}{\mu_n C_{ox} \frac{W}{L}} - {V_{in}}^2} \right) R_D \tag{3.9}$$

Using taylor series coefficients $Vout_{diff}$ can be written as:

$$Vout_{diff} = \alpha_1 V_{in} + \alpha_2 (V_{in})^2 + \alpha_3 (V_{in})^3 \tag{3.10}$$

where :

$$\alpha_1 = gm_{3,4,5,6} R_D \tag{3.11}$$

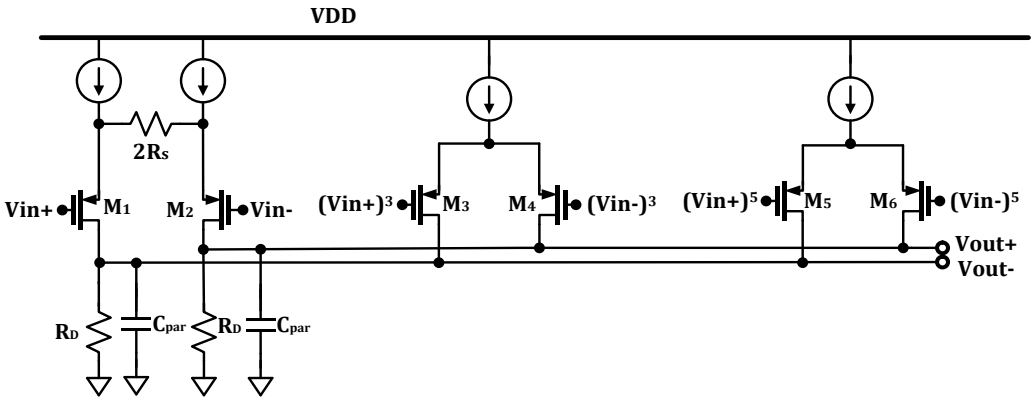

Figure 3.11: Schematic of current summer

$$\alpha_2 = 0 \tag{3.12}$$

$$\alpha_3 = -\frac{\left(\mu_n C_{ox}\frac{W}{L}\right)^2 R_D}{8gm_{3,4,5,6}} \tag{3.13}$$

The A_{IIP3} which represents the input amplitude at which the amplitude of the fundamental at the output is equal to the amplitude of the third-order intermodulation at the output is given as:

$$A_{IIP3} = \sqrt{\frac{4}{3}\left|\frac{\alpha_1}{\alpha_3}\right|} = \sqrt{6}(V_{GS0} - V_{TH}) \tag{3.14}$$

where $(V_{GS0} - V_{TH})$ is the overdrive voltage of each transistor in equilibrium. As the signal amplitude gets larger the difference between the third-order intermodulation product and the fundamental amplitude at the output gets smaller. To increase the range of inputs at which the amplitude of the fundamental is far greater than that of the intermodulation requires the input pairs to have large overdrive. In the technology used to design the predistortion circuit, the supply voltage is 1.2V so the amount of overdrive that can be given to a transistor is limited. The output of the cubic and raised to the fifth order path have small signal amplitudes so even with

overdrive of ~ 150mV the differential pairs are able to achieve the amount of linearity required such that the performance of the predistortion is not degraded much. For the main path where the signal amplitude is large, the amount of overdrive needed to achieve the linearity requirement is hard to generate with 1.2V supply. A source degenerated differential amplifier is used. Using the same analysis as before , the A_{IIP3} of a source degenerated differential pair is given as[52]:

$$A_{IIP3} = \sqrt{\frac{2gm}{3R_s}} \frac{(1 + gmR_s)^2}{\frac{1}{2}\mu_n C_{ox} \frac{W}{L}} \tag{3.15}$$

with the source degenerated resistor, the A_{IIP3} can be increased by increasing the degeneration resistor value. As the resistor value increases the transconductance /gain decreases. The source degenerated differential pair provides excellent linearity for large input signal amplitude but consumes more power to be able to generate the same gain as the non-degenerated differential pair.Fig.3.12 shows the DC gain of the summer which ideally should be 3V/V because each differential pair is designed to have a gain of 1.The DC gain achieved (3.4V/V) is slightly above the expected and has a -3dB of ~5GHz.

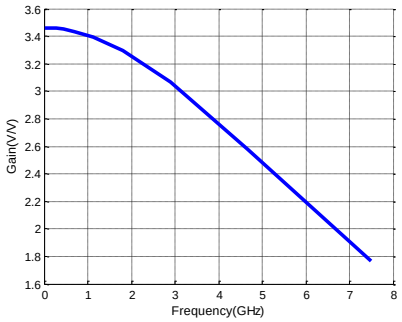

Figure 3.12: Gain of the current summer

3.2.3 Cube Generator

Several cube generators exist in the literature which have been used traditionally for the predistortion of power amplifiers (PA). Many of the earlier works made use of the non-linear impedance characteristics of back–to-back diodes[53]–[55]. Also an active using bipolar junction transistor with higher cubing gain[56]. These are not attractive as they are difficult to implement in CMOS process. CMOS cube generator has also been demonstrated in[45], [57].These cube generator heavily reduces the IM3 output signal as they take advantage of the relatively weak third-order Taylor series coefficient of the MOSFET. The cube generator Fig.3.13 is based on that presented in [58]. Unlike[58] the circuit shown in Fig.3.13 is a true cube generator not a cubic-term generator. The cubing circuit uses multiple non-linear operation to generate the cubing function (Fig.3.14). The first nonlinear operation performed is the squaring of the input signal which is done by a simple MOS squaring circuit in the lower left-bottom corner of the cube generator (Fig.3.13). The squaring circuit consist of two NMOS with their sources tied to ground and the drains connected together. The connected drains are then connected via a resistor to the

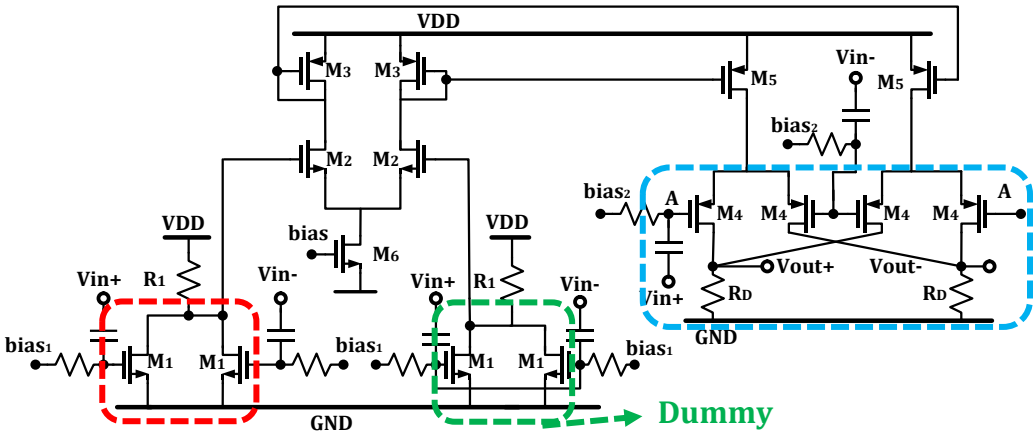

Figure 3.13: Schematic of cube generator

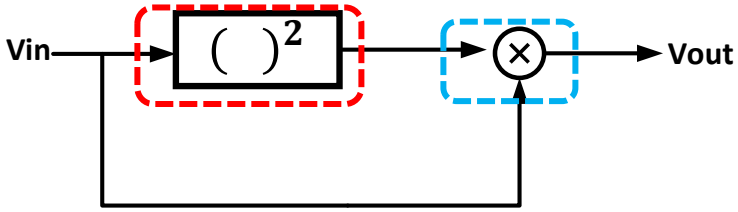

Figure 3.14: Block diagram of the operation of the cube generator

supply. The gate of the two NMOS are driven differentially. The total current flowing into the resistor is the sum of the current of the NMOS transistors. The current generated by NMOS with input V_{in+} and bias voltage V_{bias} assuming square law transistor is given by:

$$I_{D1} = \frac{1}{2}\mu_n C_{ox}\left(\frac{W}{L}\right)_1 (V_{in+} + V_{bias} - V_{th})^2 \tag{3.16}$$

$$I_{D1} = K_1 {V_{in+}}^2 + 2K_1(V_{bias} - V_{th})V_{in+} + (V_{bias} - V_{th})^2 \tag{3.17}$$

$$\text{where} \quad K_1 = \frac{1}{2}\mu_n C_{ox}\left(\frac{W}{L}\right)_1 \tag{3.18}$$

Likewise the current generated by the NMOS with input V_{in-} and bias voltage V_{bias} is given as:

$$I_{D2} = K_1 {V_{in-}}^2 + 2K_1(V_{bias} - V_{th})V_{in-} + (V_{bias} - V_{th})^2 \tag{3.19}$$

$$\text{But} \quad V_{in+} = -V_{in-} \tag{3.20}$$

The total current flowing through the resistor (I_D) which as mentioned earlier is the sum of the current of the two NMOS transistor will be given as:

$$I_D = 2K_1 {V_{in+}}^2 + 2(V_{bias} - V_{th})^2 \tag{3.21}$$

For the linear part of the current of the transistors to cancel out (3.17) and (3.19) requires proper matching of the transistors during layout. The output of the squaring circuit is single-ended so it is followed by a single-ended to differential converter to recast the signal differential. The squaring circuit directly passes the common mode signal so the negative input of the single-ended to differential converter is connected to a dummy squaring circuit. The gate terminal of the dummy squaring branch is tired together so the circuit only passes the common-mode. With that in place the common mode passed by the squaring circuit is rejected by the common rejection ratio of the single-ended to differential converter. The squared of the input signal and the input signal are multiplied together using a gilbert cell multiplier to generate the cube of the input signal. Assuming perfect symmetry between the M_2's and M_3's, the differential input voltage (V_{in}) and the differential output voltage (V_{out}) of Fig.3.13 are related by:

$$V_{out} \approx \left(\frac{gm_2}{gm_3}\sqrt{2\beta_5\beta_4}\, K_1 R_1\right) R_D {V_{in}}^3 \tag{3.22}$$

$$\text{where} \quad \beta_5 = \mu_p C_{ox}\left(\frac{W}{L}\right)_5 \tag{3.23}$$

$$\text{and} \quad \beta_4 = \mu_p C_{ox} \left(\frac{W}{L}\right)_4 \tag{3.24}$$

M_2 and M_3 sees a squared of the input signal and a gain version of the square of the input signal respectively. As the amplitude of the input signal is less than one , the squared and a gain version of the squared of the input signal are small signal so does not limit the linearity of the cube generator. The linearity of the cube generator is limited by M_4s and M_1s as they see the input signal which can be large at high modulation index. M1s have their source connected to ground so have enough overdrive so does not limit the linearity much as compared to M_4.The linearity of the cube generator is therefore increased by increasing the overdrive voltage of M_4 and M_1. Fig.3.15 shows the output characteristics of the implemented cube generator compared to an ideal cube generator with a gain. At low input signal the implemented cube generator matches the ideal cube generator. But as the input voltage get larger >200mV the implemented cube generator circuit deviates from the ideal cube generator. So there is a limitation to the input amplitude at which a true cubing function can be realized.

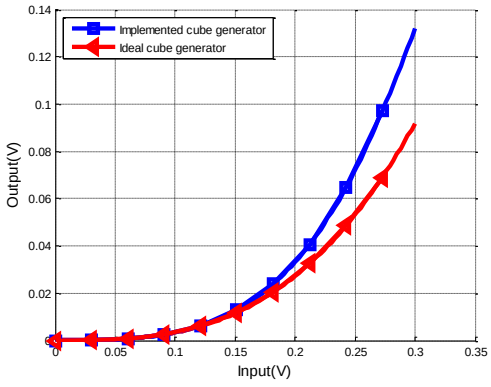

Figure 3.15: Output characteristics of the cube generator

3.2.4 Raised- To- The Fifth Generator

The block diagram and schematic of the raised-to-the fifth generator is shown in Fig.3.17 and 3.16 respectively. The raised to the fifth operation is achieved by utilizing multiple non-linear operation. Firstly, the circuit at the top part of Fig.3.16 (enclosed by the red shape) is used to obtain the square of the input signal. The configuration of M_7 and R_7 generates the square of the input. The output of the squaring circuit is single ended so the configuration of M_9 and M_{10} converts it to differential. At D+ and D- a differential square of the input signal is obtained. The circuit at the bottom of Fig3.16 (enclosed by the blue shape) is the same as the cube generator shown in Fig.3.13. It generates a differential cube of the input at C+ and C- .The gilbert cell multiplier (circuit enclosed by the green shape) is used to multiple the square of the input and the cube of the input to generate a raised- to- the fifth of the input. The differential input voltage (V_{in}) and the differential output voltage (V_{out}) of Fig.3.16 are related by:

$$V_{out} \approx \sqrt{2\beta_{11}\beta_{12}}\left(\frac{gm_2}{gm_3}\sqrt{2\beta_5\beta_4}\,K_1R_1\right)R_D\left(\frac{gm_9}{gm_{10}}\,K_7R_7\right)R_mV_{in}^{\,5} \qquad (3.25)$$

$$\text{where} \quad \beta_n = \mu_pC_{ox}\left(\frac{W}{L}\right)_n \text{ for } n = 4,5,11 \text{ and } 12 \qquad (3.26)$$

The gilbert cell multiplier (circuit enclosed by the green shape) sees the square and cubic of the input signal which are small signals so doesn't limit the linearity of the raised-to-the fifth generator by much. The gilbert cell multiplier in the cube generating part as talked about earlier has its M_4 transistors seeing the input signal which can be considerable large at high modulation index and as such limit the linearity of the raised-to-the fifth generator. The M_4 transistors of the gilbert cell multiplier are sized with large overdrives to improve the linearity of the circuit.

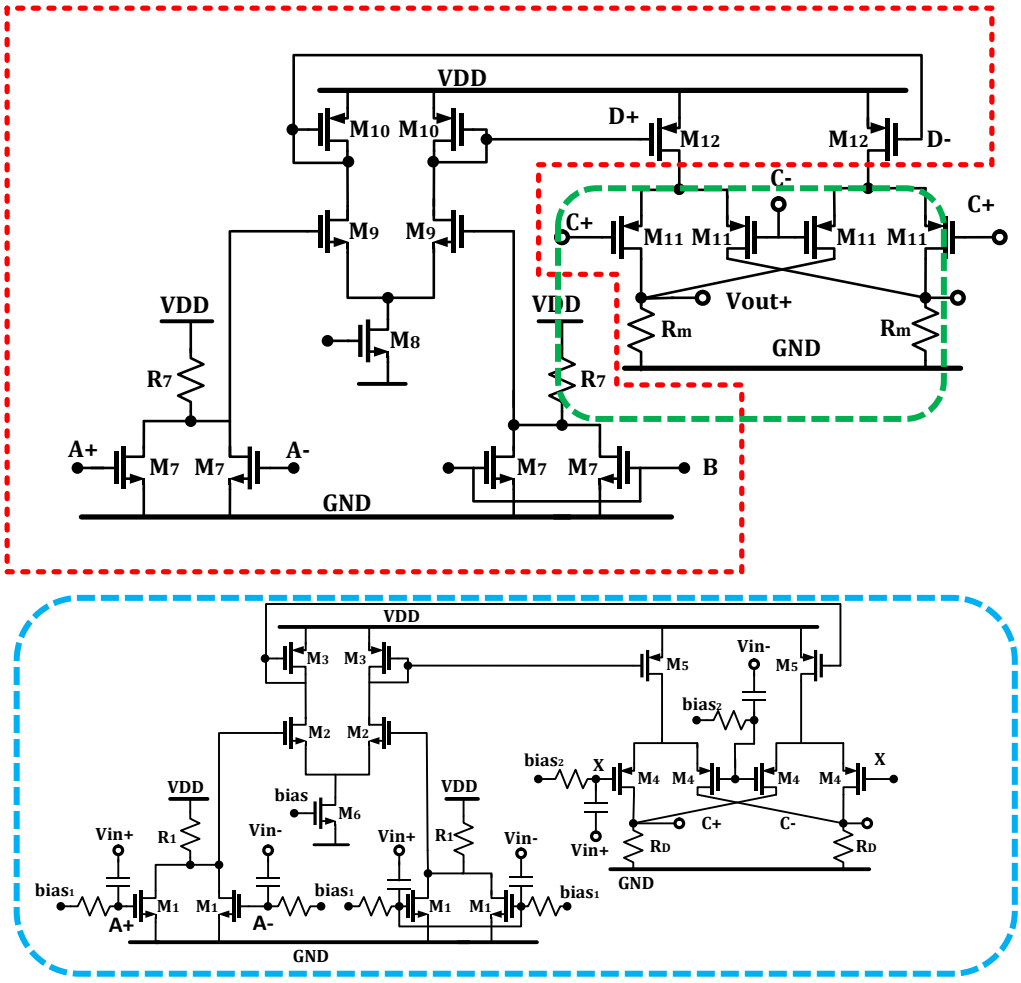

Figure 3.16: Schematic of raised-to-the fifth generator

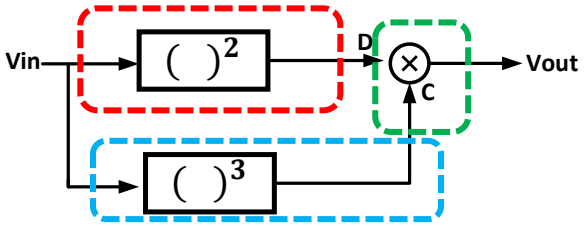

Figure 3.17: Block diagram showing the operation of the circuit.

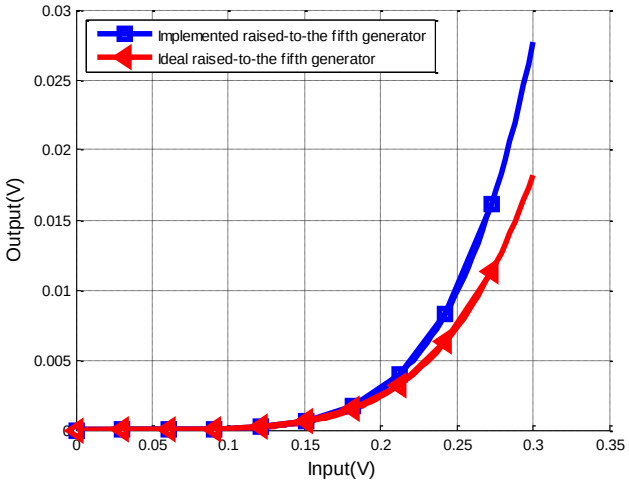

Figure 3.18: Output characteristics of raised-to-the fifth generator

Fig.3.18 shows the output characteristics of the implemented raised-to-the fifth generator compared to an ideal raised-to-the fifth generator with a gain. At low input signal the implemented raised-to-the fifth generator matches the ideal raised-to-the fifth generator. But as the input voltage get larger >230mV the implemented raised-to-the fifth generator circuit deviates from the ideal. There is a limitation to the input amplitude at which a true raised-to-the fifth function can be realized.

3.2.5 Variable Gain Amplifier (VGA)

The variable gain amplifier is shown in Fig.3.19. It consist of two differential pairs M_1, M_2 and M_3, M_4 which are cross-coupled. The linearity of the VGA is improved by source degeneration of the differential pairs. The resistor is connected across the source of the differential such that if the differential pairs are perfectly matched and the tail currents which are split into two transistors (M_7, M_8 and M_9, M_{10}) are also perfectly matched then no dc current will flow through the resistors ($2R_S$). In addition ($2R_S$) does not consume any headroom which is important for a technology node with 1.2V supply. The resistors R_D under ideal conditions, sets the gain of the circuit. The R_Ds have one of its terminals connected to each other and the gates of M_5 and M_6 whiles the other terminals are connected to the drain of M_1, M_5 and M_4 and

M_6. The advantage of this configuration is that assuming perfect matching between M_5 and M_6, R_D will carry no dc current and as such consumes no headroom. As a result, relatively large resistor size and relative large current can flow through the differential pair to achieve large gain without compromising headroom. In addition R_D provides common mode feedback for the VGA. When the common mode voltage at the drain of M_1, M_5 or M_4, M_6 start to fall/rise R_D senses the voltage and pull-down/pull-up the gate voltage of M_5 and M_6 to restore the common-mode. As the VGA is going to drive an ac-coupling network it requires a low output impedance and that is provide by M_{11}, M_{13} and M_{14}, M_{12} which forms a buffer. The voltage gain of the VGA is given as:

$$Gain = \frac{\left(\left(\frac{gm_{1,2}}{1+gm_{1,2}R_s}\right)-\left(\frac{gm_{3,4}}{1+gm_{3,4}R_s}\right)\right)}{go_{5,6}+go_{1,4}+go_{2,3}+g_D}\left(\frac{gm_{13,14}}{gm_{13,14}+go_{13,14}+go_{11,12}}\right) \quad (3.27)$$

The extra differential pair M_{17} and M_{18} is used to varying the gain of the VGA. When a differential voltage (V_{ctrl+} - V_{ctrl-}) is applied to the gates of M_{17} and M_{18} it changes the current flowing through the $M_{1,2}$ and $M_{3,4}$ by changing the voltage at A and B. Which changes their transconductance and thus the gain. Because of the source degeneration the gain tuning range achieved is relatively small and that is the trade of for using the source degeneration. This is issue is addressed by placing the VGA before the cube generator and raised-to-the fifth generator (Fig.3.7) which increases the tuning range by 3X and 5X respectively. Fig.3.20 shows how the voltage gain of the VGA varies with the control voltage. A gain range of (0.8~2) is achieved.

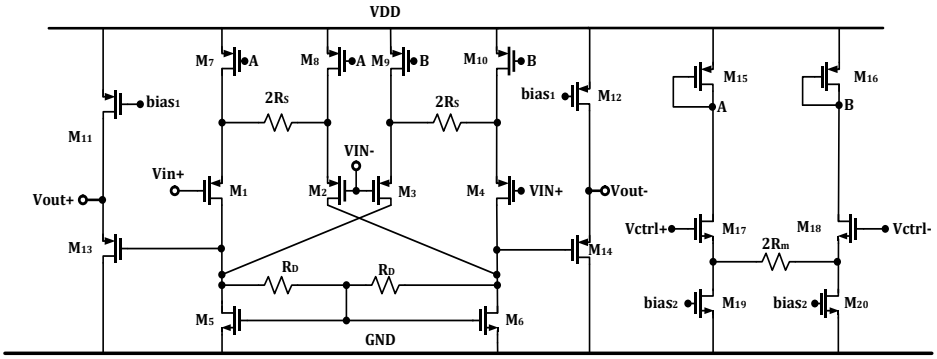

Figure 3.19: Variable gain amplifier

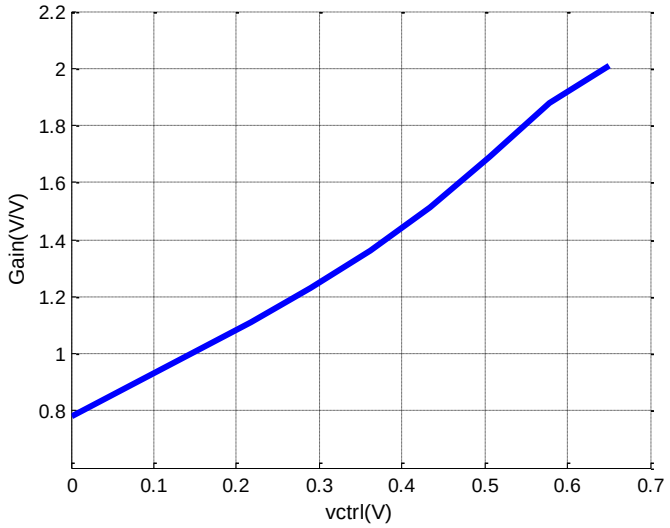

Figure 3.20: Gain vs vctrl

3.2.6 Buffer

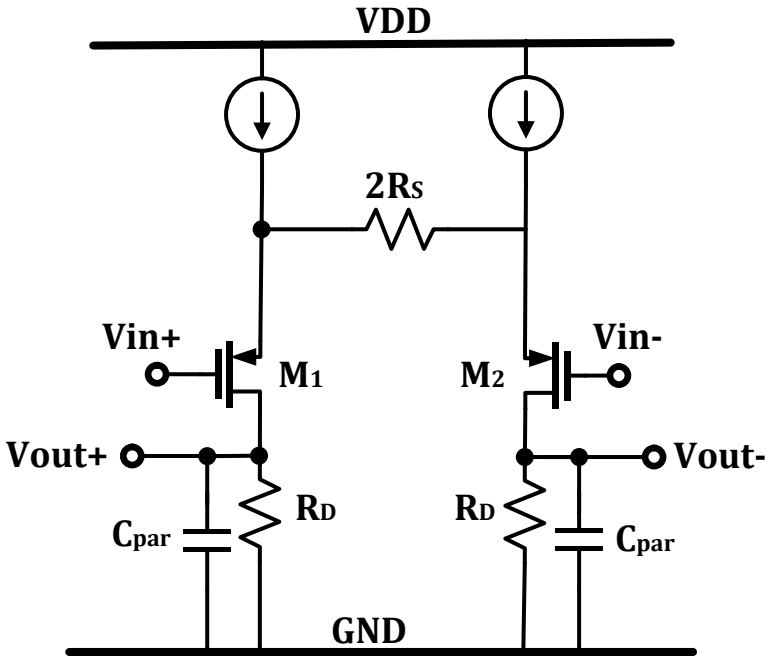

Figure 3.21: Schematic of buffer

A buffer (Fig.3.21) is needed at the output of the summer as the predistortion IC is supposed to drive an off-chip power amplifier via a 50ohm impedance trace. The resistance of the differential amplifiers are sized as 50ohm to provide 50ohm on-chip termination. As mentioned earlier, the resistor Rs is used to increase the linearity of the buffer so that it does not degrade the performance of the predistortion circuit. The voltage gain of the buffer is given as:

$$Gain(s) \approx \left(\frac{\left(\frac{gm_{1,2}}{1 + gm_{1,2}R_s} \right)}{gds_{1,2} + g_D} \right) \Bigg/ \left(1 + \frac{sC_{par}}{gds_{1,2} + g_D} \right) \tag{3.28}$$

Fig.3.22 is the voltage gain of the buffer. Ideally it should be 0.5V/V. A gain slightly above the target is achieved.

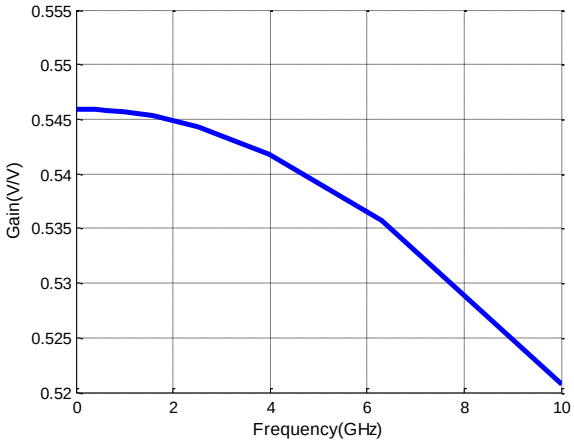

Figure 3.22: Voltage gain of the 50ohm buffer

3.3 Results

The proposed fifth-order predistortion circuit was designed and fabricated in GP TSMC 65nm CMOS technology. Fig.3.23 and 3.24 show the full chip layout of the predistortion circuit (including power supply decaps and metal fillings) and chip micrograph respectively. The chip occupies an area of 1.040mm X 1.040mm.

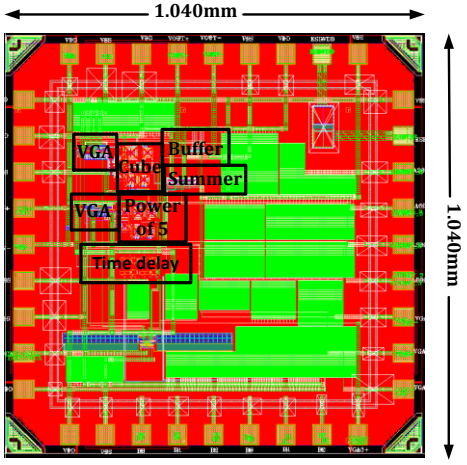

Figure 3.23: Full chip layout of the proposed predistortion

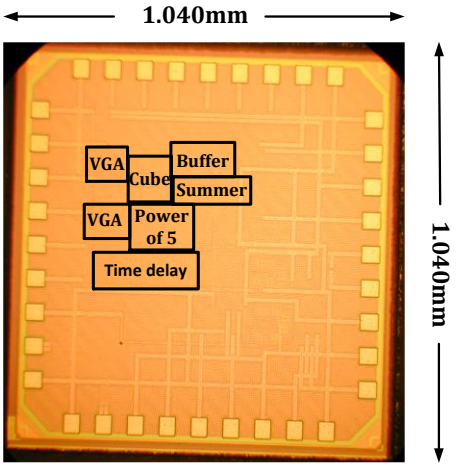

Figure 3.24: Chip micrograph of the proposed predistortion

3.3.1 Simulation Results

It can be seen in Fig.3.25 and 3.26 that without predistortion the IM3 was 31.65dBc but with predistortion it increased to 57.59dBc which means the predistortion introduced ~26dB improvement at 49.7% modulation depth with 10MHz bandwidth. At bandwidth of 100MHz and 200MHz the IM3 are 48.57dB and 43.65dB respectively, Fig.3.28 and Fig.3.30 resulting in ~21dB and ~16dB improvement for 100MHz and 200MHz bandwidth respectively. Fig.3.31 shows the improvement of IM3 with modulation depth. The improvement decreases with increasing modulation index.

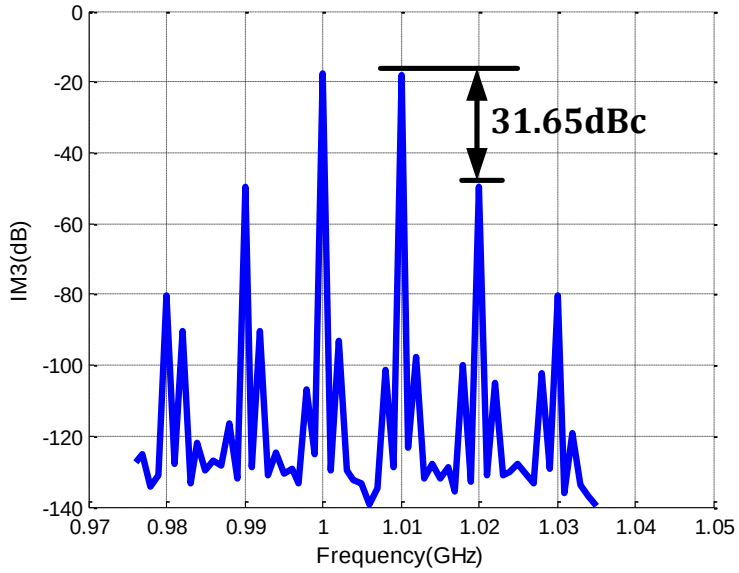

Figure 3.25: MZM output without predistortion (1GHz & 1.01GHz inputs)

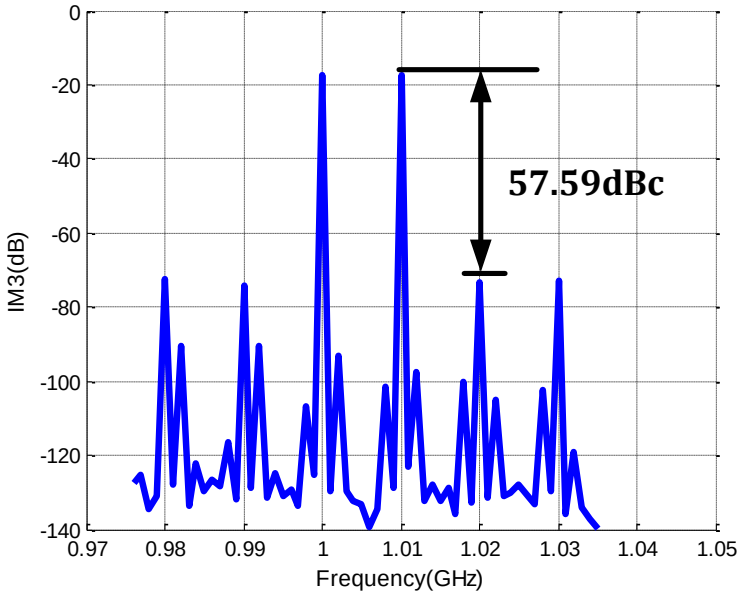

Figure 3.26: MZM output with predistortion (1GHz & 1.01GHz inputs)

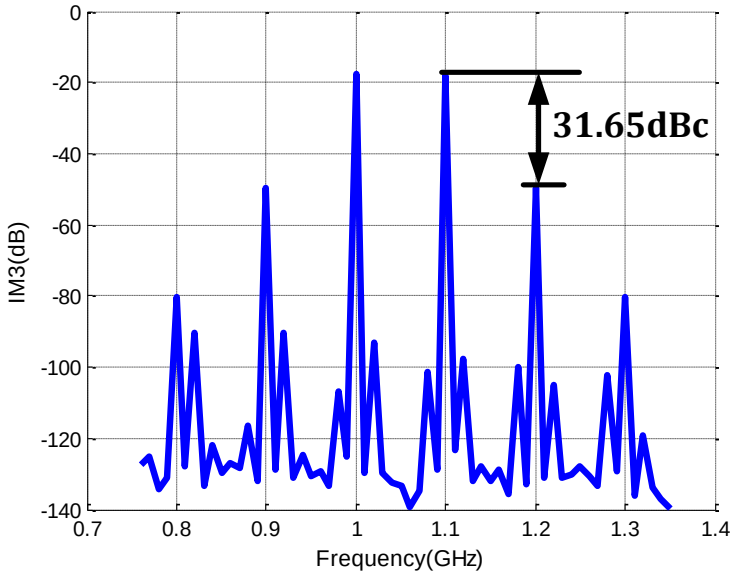

Figure 3.27: MZM output without predistortion (1GHz & 1.1GHz inputs)

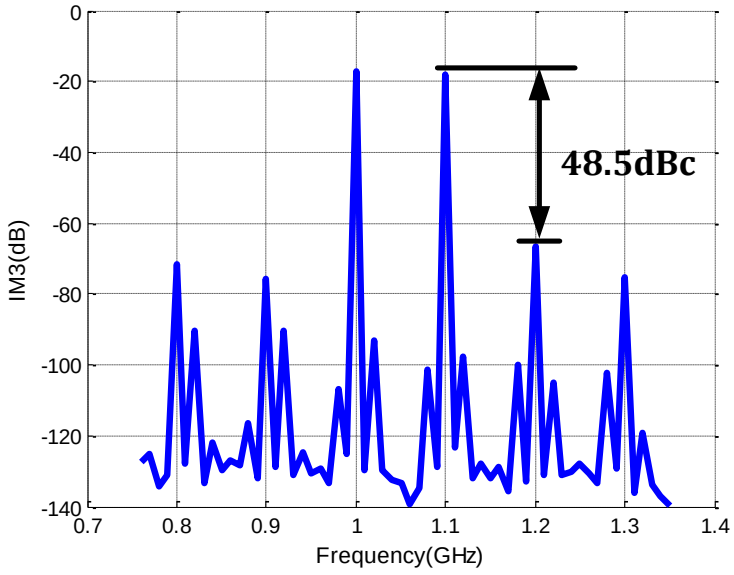

Figure 3.28: MZM output with predistortion (1GHz & 1.1GHz inputs)

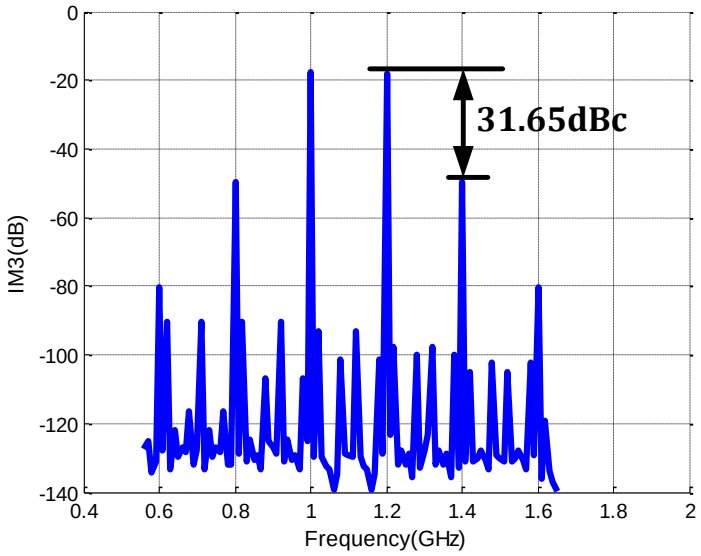

Figure 3.29: MZM output without predistortion (1GHz & 1.2GHz inputs)

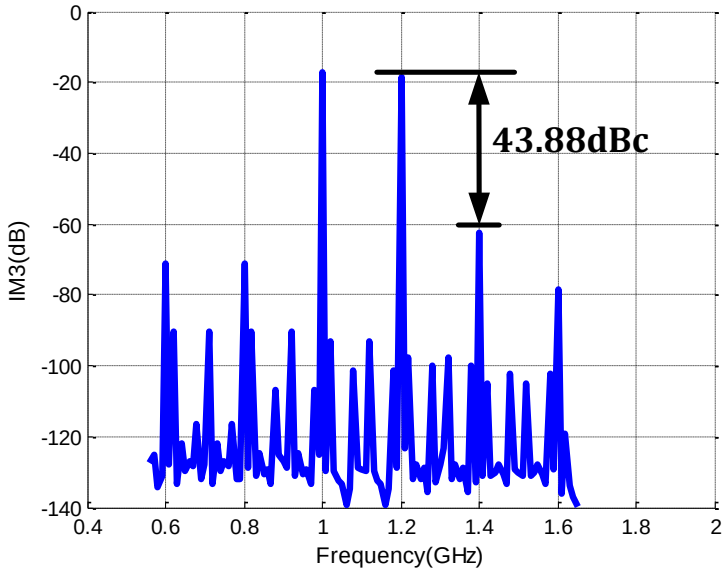

Figure 3.30: MZM output with predistortion (1GHz & 1.2GHz inputs)

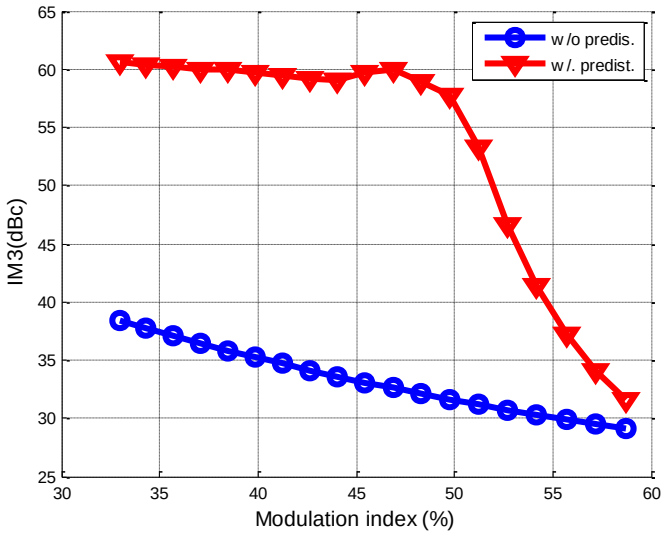

Figure 3.31: IM3 versus modulation depth

3.3.2 Experimental Results

To test the fabricated chip, two measurement are performed. Firstly, a two tone sine wave is applied to the chip and the output of the chip is saved using a real time scope. The saved output is passed through an ideal power amplifier model and a MZM matlab model and FFT is performed on the output of the MZM matlab model to see the frequency content. The MZM matlab model is obtained by performing measurement on an actual MZM module. The chip achieved 17.9dB, 23dB and 22dB for modulation depths of 40.25%, 44.5% and 49.7% respectively (Fig.3.33, Fig.3.35 and Fig.3.37). Secondly, the output of the chip is applied to the an external power amplifier and the output of the power amplifier is saved using a real time scope and then applied to the matlab MZM model. The chip achieved 12.8dB, 18dB and 20.2dB for modulation depths of 40.25%, 44.5% and 49.7% respectively (Fig.3.39, Fig.3.41 and Fig.3.43). The degradation is due to power amplifier nonlinearities. Fig.3.44 shows the summary of the experimental results

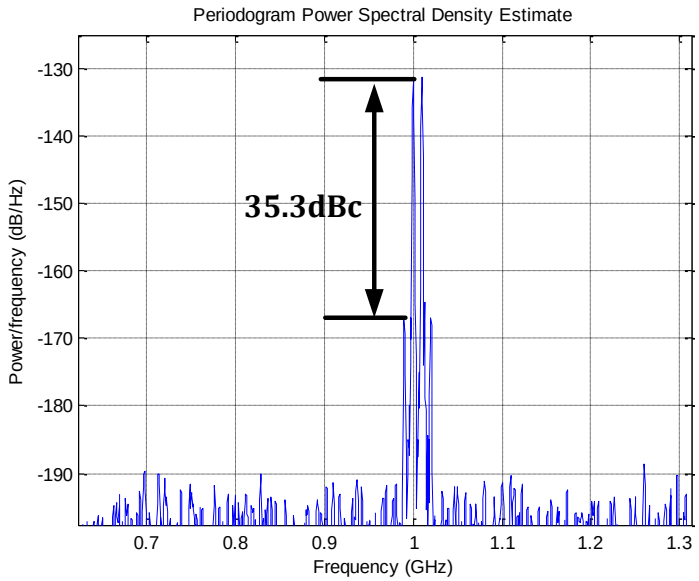

Figure 3.32: MZM output without predistortion @40.25% modulation depth

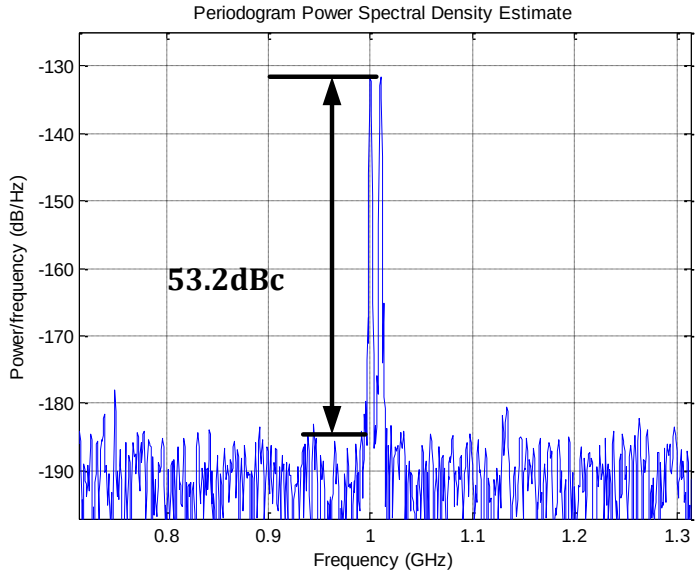

Figure 3.33: MZM output with predistortion @40.25% modulation depth

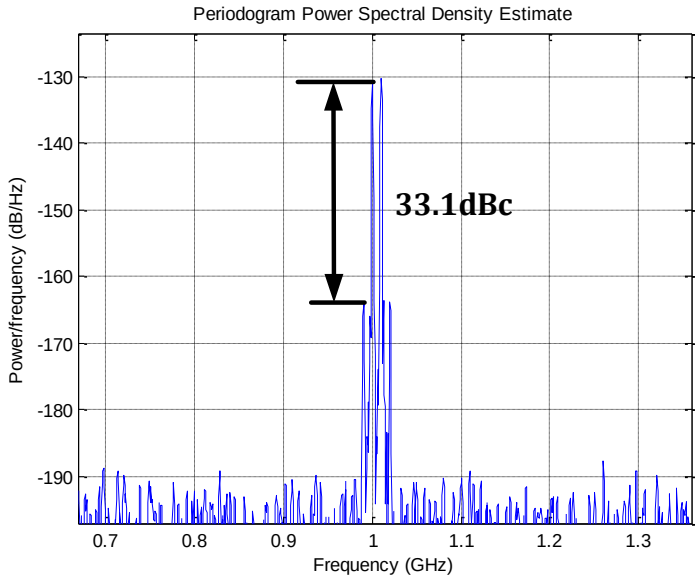

Figure 3.34: MZM output without predistortion @44.5% modulation depth

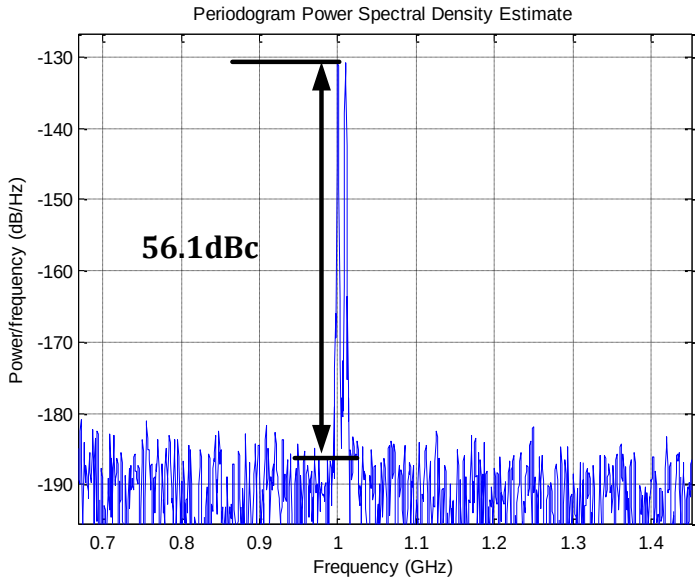

Figure 3.35: MZM output with predistortion @44.5% modulation depth

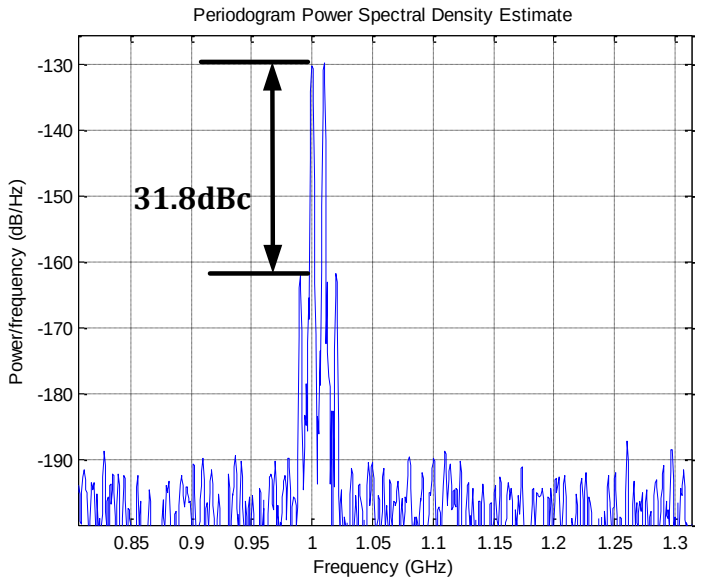

Figure 3.36: MZM output without predistortion @49.7% modulation depth

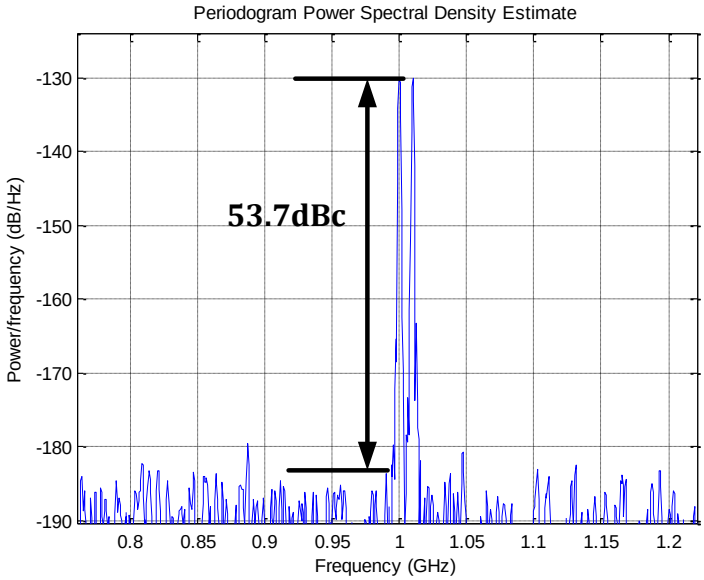

Figure 3.37: MZM output with predistortion @49.7% modulation depth

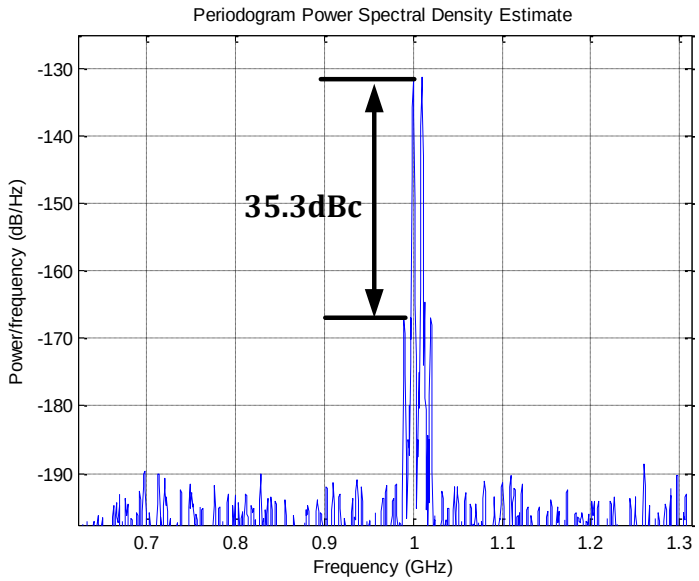

Figure 3.38: MZM output without predistortion @40.25% modulation depth

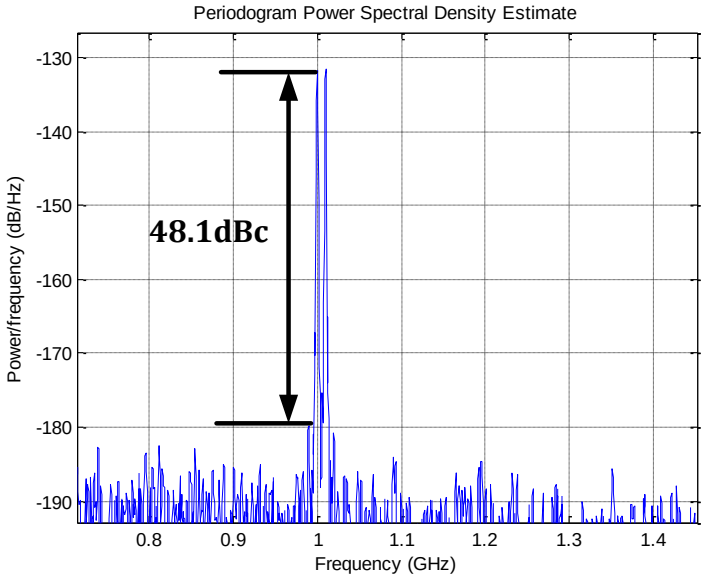

Figure 3.39: MZM output with predistortion @40.25% modulation depth

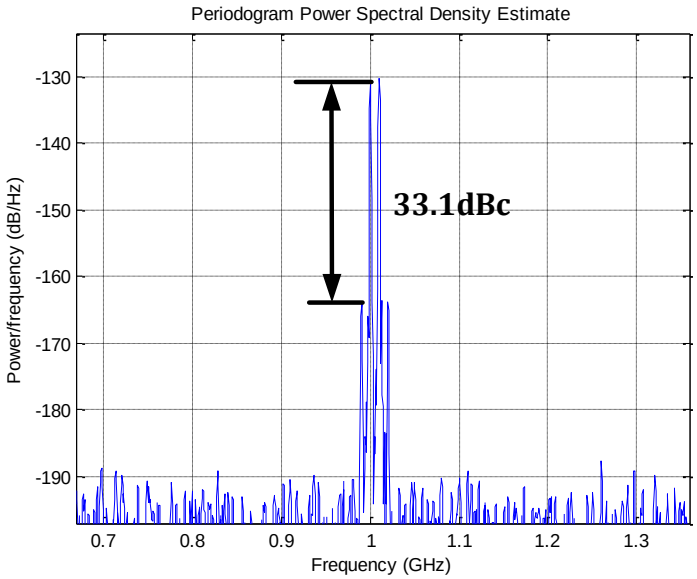

Figure 3.40: MZM output without predistortion @44.5% modulation depth

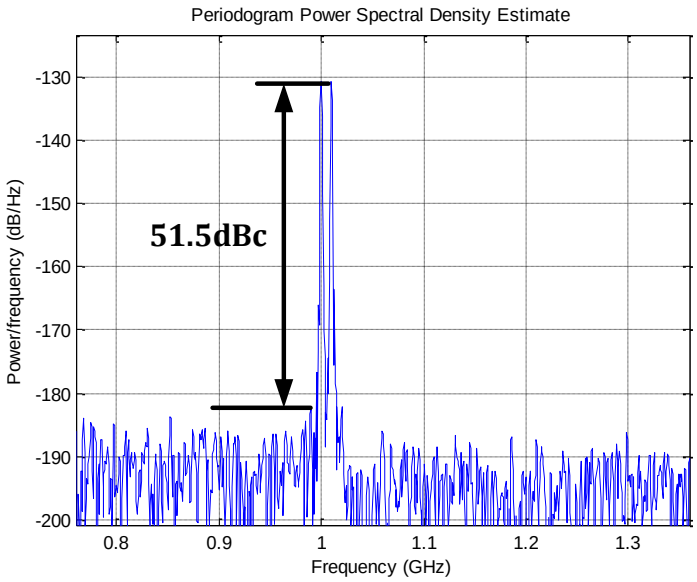

Figure 3.41: MZM output with predistortion @44.5% modulation depth

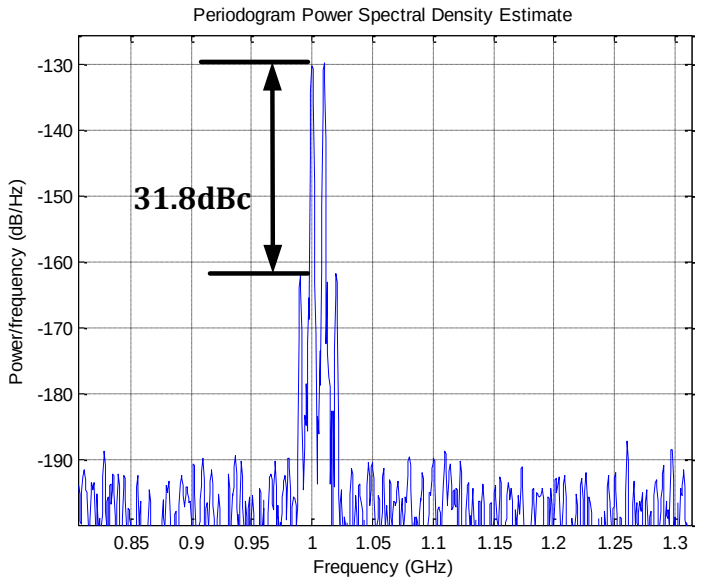

Figure 3.42: MZM output without predistortion @49.7% modulation depth

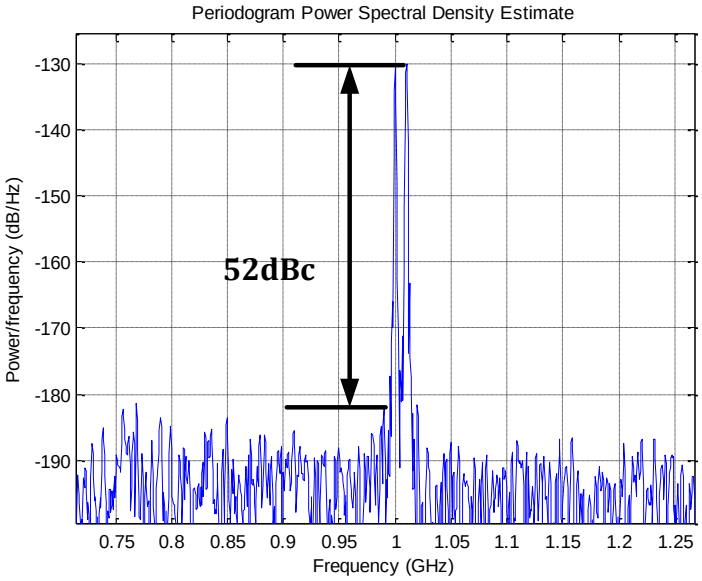

Figure 3.43: MZM output with predistortion @49.7% modulation depth

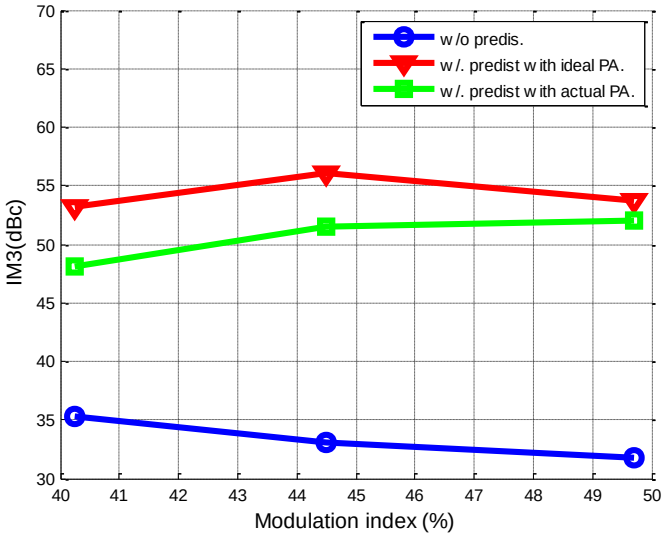

Figure 3.44: IM3 versus modulation depth

3.4 Comparison of Results

Table 1 compares the performance of the proposed fifth-order predistortion with two other electrical predistortion published works. The proposed work was able to achieve better improvement in IM3 compared to the other two works published.

Table 1: Table of Comparison

Reference	[44]	[45]	**This work**
Tech(μm)	0.6	0.18	**0.065**
Predistortion Type	5th	3rd	**5th**
I_{DD}(mA)	N/A	90	**41**
Center Frequency(GHz)	1	0.28	**1**
Modulation Depth(%)	49.6	40	**49.7**
IM3(dBc)@ 10MHz BW	17	21	**~20**

4 CONCLUSION

A fifth-order predistortion linearization of MZM has been presented that is able to achieved good IM3 suppression at high modulation depth. The polynomial coefficient of the predistortion can be independently controlled to obtain optimized suppression of both the IM3 and IM5.

The concept of the proposed solution is presented in section 3.1 and the circuit implementation and design is discussed in section 3.2. Prior to the proposed work different schemes of linearization of the MZM has also been discussed.

The proposed solution was design and fabricated in GP 65nm TSMC CMOS process and it achieves 20dB improvement in IM3 at 49.7% modulation index with 49.2mW of power consumed. This is the highest reported in the literature.

REFERENCES

[1] J. S. Rodgers, "Technologies for RF Photonics in Wideband Multifunction Systems," in *IEEE Avionics, Fiber-Optics and Photonics Conference*, 2013, vol. 1, pp. 7–8.

[2] S. A. Pappert and B. Krantz, "RF Photonics for Radar Front-Ends," in *IEEE Radar Conference*, 2007, pp. 965–970.

[3] M. S. Rasras *et al.*, "Demonstration of a Fourth-Order Pole-Zero Optical Filter Integrated Using CMOS Processes," *IEEE J. Light. Technol.*, vol. 25, no. 1, pp. 87–92, 2007.

[4] B. E. Little *et al.*, "Very High-Order Microring Resonator Filters for WDM Applications," *IEEE Photonics Technol. Lett.*, vol. 16, no. 10, pp. 2263–2265.

[5] T. Barwicz, M. A. Popovi, M. R. Watts, P. T. Rakich, E. P. Ippen, and H. I. Smith, "Fabrication of Add – Drop Filters Based on Frequency-Matched Microring Resonators," *IEEE J. Light. Technol.*, vol. 24, no. 5, pp. 2207–2218, 2006.

[6] K. Tu *et al.*, "Silicon RF-Photonic Filter and Down-Converter," *IEEE J. Light. Technol.*, vol. 28, no. 20, pp. 3019–3028, 2010.

[7] L. Pavesi and G. Guillot, *Optical Interconnects:The Silicon Approch*. Berlin: Springer, 2006.

[8] G. Mashanovich, F. Y. Gardes, G. T. Reed, and D. J. Thomson, "Silicon Optical Modulators," *Nat. Photonics*, vol. 4, no. 8, pp. 518–526, 2010.

[9] E. Sackinger, *Broadband Circuits for Optical Fiber Communication*. Hoboken, New Jersey: John Wiley & Sons, Inc, 2005.

[10] H. H. Q. Bossert David J., Collins Doug, Aeby Ian, Clevenger J. Bridget, Helms Christopher J., Luo Wenlin, Wang Charlie X, "Production of High-Speed Oxide-Confined VCSEL Arrays for Datacom Applications," *SPIE*, vol. 4649, pp. 142–

151, 2002.

[11] C. H. Cox, *Analog Optical Links Theory and Practice*. Cambridge, New York: Cambridge University Press, 2004.

[12] T. L. Koch, "Laser Sources for Amplified and WDM Lightwave Systems," in *Optical Fiber Telecommunications IIIB*, San Diego: Academic Press, 1997, pp. 115–162.

[13] D. A. Fishman and B. S. Jackson, "Transmitter and Receiver Design for Amplified Lightwave Systems," in *Optical Fiber Telecommunications IIIB*, San Diego: Academic Press, 1997, pp. 69–114.

[14] Welstand R, "High Linearity Modulation and Detection in Semiconductor Electroabsorption Waveguides," Ph.D. dissertation, University of California, San Diego, 1997.

[15] S. k. Halemane, T.R. and Korotky, "Distortion Characteristics of Optical Directional Coupler Modulators," in *IEEE Trans. Microwave Theory Tech.*, 1990, pp. 669–673.

[16] D. Rabus, *Integrated Ring Resonators: The Compendium*. Berlin: Springer, 2007.

[17] Q. Xu, B. Schmidt, S. Pradhan, and L. Michal, "Micrometre-Scale Silicon Electro-Optic Modulator," *Nature*, vol. 435, no. 7040, pp. 325–327, 2005.

[18] S. Dubovitsky, W. H. Steier, L. Fellow, S. Yegnanarayanan, B. Jalali, and S. Member, "Analysis and Improvement of Mach – Zehnder Modulator Linearity Performance for Chirped and Tunable Optical Carriers," *IEEE J. Light. Technol.*, vol. 20, no. 5, pp. 886–891.

[19] B. H. Kolner and D. W. Dolfi, "Intermodulation Distortion and Compression in an Integrated Electrooptic Modulator," *Appl. Opt.*, vol. 26, no. 17, pp. 3676–3679, 1987.

[20] K. Noguchi, H. Miyazawa, and O. Mitomi, “Frequency Response of a Travelling Wave Mach-zehnder Modulator,” in *Electron. Lett*, 1994, pp. 949–951.

[21] M. R. Reshotko, D. L. Kencke, and B. Block, “High-Speed CMOS-Compatible Photodetectors for Optical Interconnects,” *Soc. Photo-Optical Instrum. Eng. Conf. Ser.*, vol. 5564, pp. 146–155, 2004.

[22] Samuel Palermo PhD, “Optical Interconnects Circuits and Systems,” in *Lecture notes*, 2016, p. 33.

[23] G. E. Betts, C. H. Cox, and K. G. Ray, “20GHz Optical Analog Link Using an External Modulator,” *IEEE Photonics Technol. Lett.*, vol. 2, pp. 923–925, 1990.

[24] M. Taher, “Harmonic and Intermodulation Performance of Dual- Electrode Mach-Zehnder Electro-Optic Modulators with Multicarrier RF Input,” *17th Int. Conf. Telecommun.*, pp. 528–533, 2010.

[25] B. Hraimel, M. O. Twati, and K. Wu, “Closed-Form Dynamic Range Expression of Dual-Electrode Mach-Zehnder Modulator in Radio-Over-Fiber WDM System,” *IEEE J. Light. Technol.*, vol. 24, no. 6, pp. 2380–2387, 2006.

[26] G. E. Betts, “Linearizated Modulator for Suboctave-Bandpass Optical Analog Links,” *IEEE Trans. Microw. Theory Tech.*, vol. 42, pp. 2642–2649, 1994.

[27] D. J. M. Sabido, M. Tabara, T. K. Fong, C. Lu, and L. G. Kazovsky, “Improving the Dynamic Range of a Coherent AM Analog Optical Link Using a Cascaded Linearized Modulator,” *IEEE Photonics Technol. Lett.*, vol. 7, no. 7, pp. 813–815, 1995.

[28] G. E. Betts and F. J. O. Donnell, “Suboctave Linearized : Modulators,” *IEEE Photonics Technol. Lett.*, vol. 8, no. 9, pp. 8–10, 1996.

[29] W. K. Bums, “Linearized Optical Modulator with Fifth Order Correction,” *IEEE J. Light. Technol.*, vol. 13, no. 8, pp. 11–14, 1995.

[30] L. M. Johnson and H. V Roussell, “Linearization of an Interferometric Modulator at Microwave Frequencies by Polarization Mixing,” *IEEE Photonics Technol. Lett.*, vol. 2, no. 11, pp. 810–811, 1990.

[31] L. M. Johnson and H. V Roussell, “Reduction of Intermodulation Distortion in Interferometric Optical Modulators,” *Opt. Lett.*, vol. 13, no. 10, pp. 928–930, 1988.

[32] W. B. Bridges and J. H. Schaffner, “Distortion in Linearized Electro-optic Modulators,” *IEEE Trans. Microw. Theory Tech.*, vol. 33, no. 9, pp. 2184–2197, 1995.

[33] S. K. Korotky, “Dual Parallel Modulation Schemes for Low-Distortion Analog Optical Transmission,” *IEEE J. Sel. Areas Commun.*, vol. 8, no. 7, 1990.

[34] J. L. Brooks, G. S. Maurer, and R. A. Becker, “Implementation and Evaluation of a Dual Parallel Linearization System for AM-SCM Video Transmission,” *IEEE J. Light. Technol.*, vol. 11, no. 1, pp. 34–41, 1993.

[35] B. B. Dingel, “Ultra-linear , Broadband Optical Modulator for High Performance Analog Fiber Link System,” *IEEE Microw. Photonics*, pp. 0–3, 2004.

[36] X. Xie, J. Khurgin, J. Kang, and F. Chow, “Linearized Mach-Zehnder Intensity Modulator,” *IEEE Photonics Technol. Lett.*, vol. 15, no. 4, pp. 531–533, 2003.

[37] P. S. C. N.Rengand, I. Shpantzer, Ya. Achiam, A. Kaplan, A. Greenbalatt, G. Hartson, “Novel Design for the Broadband Linearized Optical Modulator,” *IEEE Mil. Commun. Conf.*, vol. 2, pp. 1208–1212, 2003.

[38] E. I. Ackerman, “Broad-Band Linearization of a Mach-Zehnder Electrooptic Modulator,” *IEEE Trans. Microw. Theory Tech.*, vol. 47, no. 12, pp. 2271–2279, 1999.

[39] S. R. O. Connor, T. R. Clark, and S. Member, “Wideband Adaptive Feedforward

Photonic Link," *IEEE J. Light. Technol.*, vol. 26, no. 15, pp. 2810–2816, 2008.

[40] T. Ismail, C. Liu, J. E. Mitchell, and A. J. Seeds, "High-Dynamic-Range Wireless-Over-Fiber Link Using Feedforward Linearization," *IEEE J. Light. Technol.*, vol. 25, no. 11, pp. 3274–3282, 2007.

[41] M. Nazarathy, J. Berger, A. J. Ley, I. M. Levi, and Y. Kagan, "Progress in Externally Modulated AM CATV Transmission Systems," *IEEE J. Light. Technol.*, vol. 11, pp. 82–105, 1993.

[42] R. B. Childs and V. A. O'Byrne, "Multichannel AM Video Transmission Using a High-Power Nd:YAG Laser and Linearized External Modulator," *IEEE J. Selec. Areas Commun.,* vol. 8, no. 7, pp. 1369–1376, 1990.

[43] L. Zhang *et al.*, "Ten-GHz MMIC Predistortion Circuit for Improved Dynamic Range of Broadband Analog Fiber-Optic Link," *Microw. Opt. Technol. Lett.*, vol. 11, no. 6, pp. 293–295, 1996.

[44] Y. Chiu, B. Jalali, S. Garner, and W. Steier, "Broad-Band Electronic Linearizer for Externally Modulated Analog Fiber-Optic Links," *IEEE Photonics Technol. Lett.*, vol. 11, no. 1, pp. 48–50, 1999.

[45] R. Sadhwani and B. Jalali, "Adaptive CMOS Predistortion Linearizer for Fiber-Optic Links," *IEEE J. Light. Technol.*, vol. 21, no. 12, pp. 3180–3193, 2003.

[46] F.Ellinger, "Passive Devices and Networks," in *Radio Frequency Integrated Circuits and Technolgies*, Berlin: Springer, 2007, pp. 195–198.

[47] F. E. van Vliet, M. van Wanum, A. W. Roodnat, and M. Alfredson, "Fully-Integrated Wideband TTD Core Chip With Serial Control," in *Gallium Arsenide Applications Symp.*, 2003, pp. 89–92.

[48] T. Chu, J. Roderick, and H. Hashemi, "An Integrated Ultra-Wideband Timed Array Receiver in 0.13 um CMOS Using a Path-Sharing True Time Delay

Architecture," *IEEE J. SolidState Circuits*, vol. 42, no. 12, pp. 2834–2850, 2007.

[49] B. Razavi, *Design of Analog CMOS integrated Circuits*. New York: McGraw-Hill, 2001.

[50] S. K. Garakoui, E. A. M. Klumperink, B. Nauta, and F. E. Van Vliet, "Compact Cascadable Gm-C All-Pass True Time Delay Cell With Reduced Delay Variation Over Frequency," *IEEE J. SolidState Circuits*, vol. 50, no. 3, pp. 693–703, 2015.

[51] S. K. Garakoui, E. A. M. Klumperink, B. Nauta, and E. Frank, "Frequency Limitations of First-Order Gm-RC All-Pass Delay Circuits," *IEEE Trans. Circuits Syst.*, vol. 60, no. 9, pp. 572–576, 2013.

[52] B. Razavi, *RF Microelectronics*, Second. New York: Paul Boger, 2012.

[53] T. Nojima and N. Konno, "Cube Predistortion Linearizer for Relay Equipment in 800MHz Band Land Mobile Telephone System," *IEEE. Trans. Veh. Technol.*, vol. 34, no. 4, pp. 169–177, 1985.

[54] N. Imai, T. Nojima, and T. Murase, "Novel Linearizer Using Balanced Circulators and Its Application to Multilevel Digital," *IEEE Trans. Microw. Theory Tech.*, vol. 37, no. 8, pp. 1237–1243, 1989.

[55] W. Huang and R. E. Saad, "Novel Third-Order Distortion Generator with Residual IM2 Suppression Capabilities," *IEEE Trans. Microw. Theory Tech.*, vol. 46, no. 12, pp. 2372–2382, 1998.

[56] L. Roselli, V. Borgioni, V. Palazzari, and F. Alimenti, "An Active Cuber Circuit for Power Amplifier Analog Predistortion," in *33rd Eur. Microw.Conf*, 2003, pp. 1219–1222.

[57] F. Shearer, "A Precision CMOS Analog Cubing Circuit," in *IEEE NEWCAS*, 2004, pp. 20–23.

[58] E. A. Keehr, S. Member, and A. Hajimiri, "Analysis of Internally Bandlimited

Multistage Cubic-Term Generators for RF Receivers," *IEEE Trans. Circuits Syst.*, vol. 56, no. 8, pp. 1758–1771, 2009.